

# Synthesis and Biological Evaluation of a c(RGDyK) Peptide Conjugate of SRPIN803

George Leonidis, Panagiotis Dalezis, Dimitrios Trafalis, Dimitris Beis, Panagiota Giardoglou, Anastasia Koukiali, Ioanna Sigala, Eleni Nikolakaki, and Vasiliki Sarli\*



Cite This: *ACS Omega* 2021, 6, 28379–28393



Read Online

ACCESS |



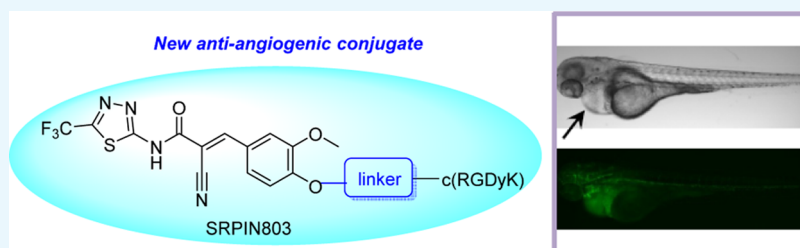
Metrics & More



Article Recommendations



Supporting Information



**ABSTRACT:** In the present study, SRPIN803 and c(RGDyK)-SRPIN803 hybrid compounds were efficiently synthesized and evaluated for their stability in human plasma and buffers of pH 7.4 and 5.2. The hybrids were mainly cytostatic against a panel of tested cancer cells, whereas one c(RGDyK)-SRPIN803 hybrid, geo35, was the most active compound in this screen and was cytotoxic against cell lines MCF7 and MRC5 with  $IC_{50}$  values of 61 and 63  $\mu$ M, respectively. SRPIN803 and geo35 exhibited antiangiogenic activity in zebrafish embryos, and this effect was dose-dependent. Although c(RGDyK)-SRPIN803 hybrid compounds were found less potent compared to SRPIN803, they have shown activities interesting enough to illustrate the potential of this approach for the development of a new class of antiangiogenic compounds.

## INTRODUCTION

Angiogenesis is defined as the formation of new blood vessels for the transport of nutrients and oxygen to cells. In normal physiology, it is a vital process that affects the migration, growth, and differentiation of endothelial cells in healing, reproduction, and growth of tissues.<sup>1</sup> The whole event is dynamic and complex involving a number of cellular and molecular interactions with the extracellular environment. Abnormal angiogenesis has been observed in cancer and other diseases such as rheumatoid arthritis, diabetic retinopathy, systemic lupus erythematosus, psoriasis, macular degeneration, and atherosclerosis.<sup>2–5</sup> Angiogenesis is stimulated by angiogenic factors such as vascular endothelial growth factor (VEGF) that has a prominent role in endothelial cell proliferation and survival, migration, and invasion of endothelial cells through the activation of its cell surface receptor VEGF receptor (VEGFR).<sup>6</sup> Apart from growth factors, cell–matrix interactions and intracellular signaling pathways are also involved in angiogenesis. For example, integrins bind extracellular matrix ligands such as vitronectin, fibronectin, fibrinogen, laminin, and collagen with the tripeptide sequence RGD.<sup>7</sup> Early studies by Soldi et al. have established that integrins  $\alpha_v\beta_3$  associate and activate VEGFR2 when endothelial cells are bound to the  $\alpha_v\beta_3$  ligand vitronectin and fibrinogen, resulting in cell migration and angiogenesis.<sup>8</sup>

Anti-VEGF inhibitors have been explored for their activities against cancer and other angiogenesis-related diseases. They

have also revolutionized the treatment of various pathologies such as age-related macular degeneration, retinal vein occlusion, or diabetic retinopathy.<sup>9</sup> An alternative approach of blocking VEGF signaling is by regulating alternative splicing. In this process, serine–arginine protein kinase 1 (SRPK1) is involved in the phosphorylation of SR splicing factors, thus controlling VEGF-mediated angiogenesis.<sup>10</sup> Consequently, a number of SRPK1 inhibitors are investigated as potential compounds for the treatment of angiogenic-related diseases. In 2006, Hagiwara et al. identified SRPIN340 as a potent SRPK1 inhibitor with a  $K_i$  value of 0.89  $\mu$ M.<sup>11</sup> Bates et al. showed that SRPIN340 reduces proangiogenic VEGF isoforms, prevents angiogenesis *in vivo*, and inhibits neovascularization in a rodent model of retinopathy of prematurity (ROP).<sup>12</sup> Later, Hagiwara and co-workers reported the discovery of another SRPK1 inhibitor, SRPIN803.<sup>13</sup> SRPIN803 inhibited the production of VEGF due to the dual inhibition of SRPK1, and CK2 and was effective in preventing age-related macular degeneration in a mouse model. CK2 is abnormally expressed in rapidly proliferating cells

**Received:** August 23, 2021

**Accepted:** October 4, 2021

**Published:** October 14, 2021



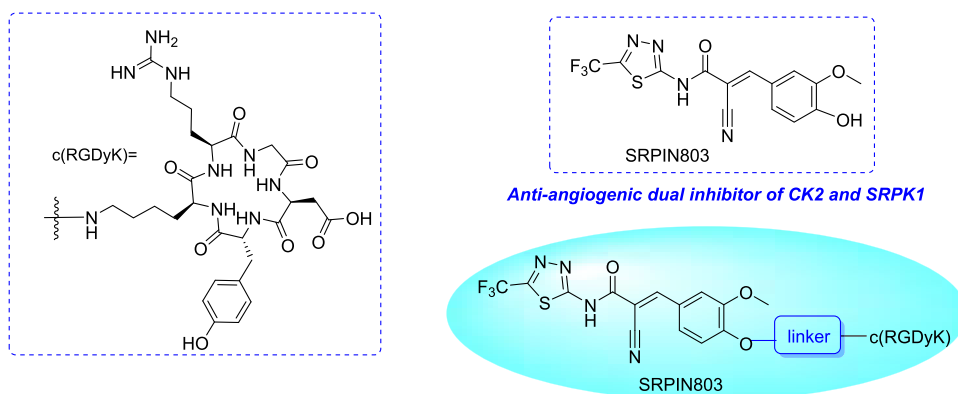
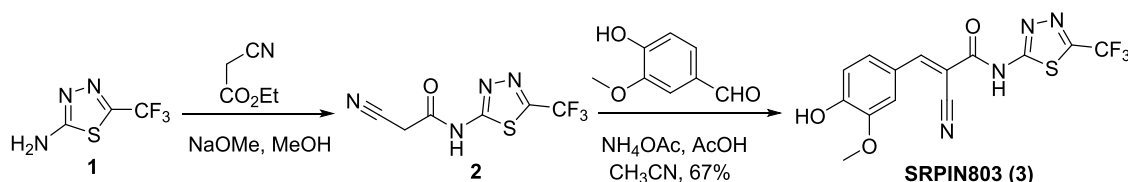
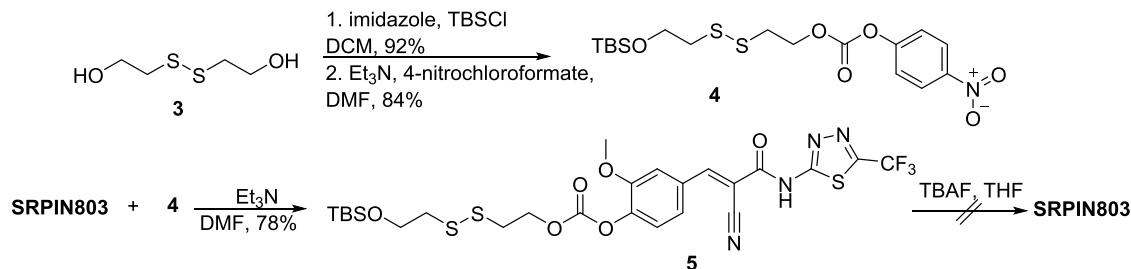


Figure 1. Structure of SRPIN803-c(RGDyK) conjugates.

### Scheme 1. Synthesis of SRPIN803



### Scheme 2. Synthesis of SRPIN803 Derivative Bearing a Carbonate Linker



and various cancer cells and is also involved in angiogenesis and neovascularization.<sup>14,15</sup>

Our group has employed cyclic pentapeptide c(RGDyK), an integrin  $\alpha_v\beta_3$  binder, for the targeted delivery of various anticancer drugs. We have observed promising anticancer activities after conjugation of triterpenoids cucurbitacins or platinum complexes to c(RGDyK).<sup>16,17</sup> Herein, we aimed to develop new antiangiogenic compounds based on the SRPK1 inhibitor SRPIN803. For this purpose, we have coupled SRPIN803 with c(RGDyK) and studied the properties of the new hybrid compounds. Different linkers were used for the attachment of the SRPIN803 on the peptide, generating specific features of the resulting conjugate (e.g., different mechanism of SRPIN803 release inside cells, hydrophobicity, stability) (Figure 1). The present work presents our efforts for the synthesis of the new hybrids and their stabilities in DMEM, different pH values, and human plasma. Furthermore, we have measured the cytotoxicity of SRPIN803 conjugates against various cell lines and inhibitory activities of key compounds against SRPK1 and CK2 kinases. The efficacy of the compounds to inhibit angiogenesis *in vivo* was estimated using zebrafish, a very useful model to study cardiovascular development.<sup>18</sup> Zebrafish intersegmental vessel angiogenesis provides the advantages of stereotypic development in combination with the ability to apply compounds at different stages of development and do noninvasive imaging. In addition, the use of the transgenic line

*Tg(kdrl:GFP)* that labels all endothelial/endocardial cells<sup>19</sup> allows the quantification of angiogenesis inhibition by any given compound.<sup>20</sup>

## RESULTS

**Design and Synthesis of SRPIN803-c(RGDyK) Conjugates.** The synthesis of SRPIN803 was performed according to Hagiwara et al. starting from 2-amino-5-(trifluoromethyl)-1,3,4-thiadiazole (1).<sup>13</sup> During our studies, Lolly and co-workers reported the revision of SRPIN803 structure proposed by Hagiwara using FT-IR spectroscopy and X-ray analysis and revised its chemical structure to 3.<sup>21</sup> In our hands, compound 1 reacted with ethyl cyanoacetate and sodium methoxide to give amide 2, which was subjected to a Knoevenagel condensation with vanillin in the presence of ammonium acetate and acetic acid. SRPIN803 was isolated as a yellow solid in 67% yield. The recorded data support the structure of a monocyclic thiadiazolopyridone (3) with the stereochemistry of SRPIN803 to be as depicted in Scheme 1.

Three different strategies for linking SRPIN803 to c(RGDyK) peptide were examined. The first approach includes the use of a noncleavable ether linker, the second a carbonate linker, and the third a primary or a secondary carbamate. Our first efforts to couple SRPIN803 with c(RGDyK) peptide by a carbonate group were unsuccessful. Initially, 2,2'-dithiodiethanol was monoprotected with *tert*-butyldimethylsilyl chloride and

activated with 4-nitrochloroformate to give the active intermediate **4** (Scheme 2). SRPIN803 reacted with compound **4** to give the desired carbonate **5** in 78% yield. Treatment of **5** with TBAF or acid for the deprotection of the TBS group showed release and cleavage of the carbonate bond. For this reason, the stability of **5** was investigated in two different pH values at 37 °C in a physiological pH 7.4 and an acidic pH 5.2. Aliquots were taken at certain time intervals and analyzed by LC–MS to estimate the stability of the carbonate ester formed by the phenol of SRPIN803 and study the release speed of SRPIN803 (Figure 2). Compound **5** was gradually hydrolyzed

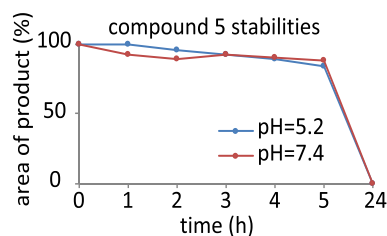


**Figure 2.** Chemostability of **5** by LC-MS analysis (results are presented as mean  $\pm$  SD for three independent experiments).

in both pH values, and after 24 h, the entire quantity was converted into its parent starting material SRPIN803. This behavior agrees with the rapid hydrolysis of **5** during the deprotection step of the silyl group.

In another experiment, c(RGDyK) peptide was attached to the drug connected via a carbamate functionality. Activation of kinase inhibitor SRPIN803 with 4-nitrophenyl chloroformate and triethylamine produced the unstable intermediate **6** that reacted further with the amino group of the lysine residue of the pentapeptide c(RGDyK) under basic conditions (Scheme 3). After 1 day, ESI-LCMS indicated the presence of product peak **7** in the mixture, while a considerable amount of **6** was converted back to its starting material SRPIN803. All attempts to isolate conjugate **7** were unsuccessful, and the carbamate ester was hydrolytically unstable (Figure 3). To study the hydrolytic behavior of carbamate derivatives of SRPIN803 and search for alternative ways to attach c(RGDyK), carbamate **9** was synthesized. Deprotection of the *tert*-butyloxycarbonyl protecting group under acidic conditions after treatment with TFA was

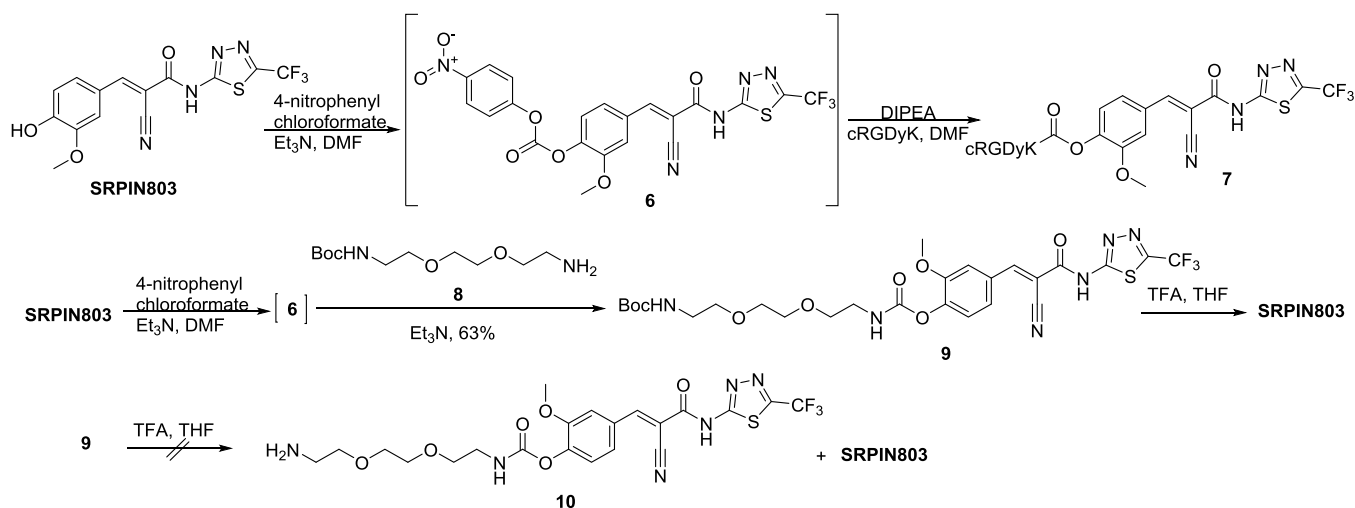
also problematic, and SRPIN803 was formed in the reaction mixture. The hydrolysis of derivative **9** at pH 7.4 and 5.2 was also studied. The conjugate maintained its carbamate ester unhydrolyzed for 2 days (>50% of its concentration stable) in acidic pH 5.2, while rapid hydrolysis was achieved after 1 h of incubation in physiological pH (Figure 3). These experiments highlight the poor stability of **9** at pH 7.4 and lead to the conclusion that a primary carbamate ester seems unsuitable to use for SRPIN803 conjugation.

To achieve a better stability profile for SRPIN803 derivatives, SRPIN803 was conjugated to c(RGDyK) using a secondary carbamate linker (Scheme 4). Starting from piperazine, we were able to obtain *N*-BOC-piperazine, which was then reacted with **6** to give carbamate **12**. Further, Boc deprotection after treatment with TFA and reaction with bis(2,5-dioxopyrrolidin-1-yl)-glutarate **15** gave derivative **16**. This compound was then coupled to the  $\epsilon$ -amino group of lysine on c(RGDyK) pentapeptide. Conjugate geo41 was isolated in 47% yield after HPLC purification and purity greater than 96%.

In a following step, our efforts were focused on the synthesis of an SRPIN803 derivative that is more stable in hydrolysis ether linker. The synthesis of geo35 conjugate is summarized in Scheme 5. The intermediate alkyl iodide derivative **S2** (2-((2-((*tert*-butyldimethylsilyloxy)ethyl)disulfanyl)ethyl (4-nitrophenyl) carbonate) was prepared from commercially available triethylene glycol following up a two-step sequence. Specifically, triethylene glycol was mesylated and subsequently reacted with sodium iodide to produce iodide **S2** in 90% overall yield, which further reacted with SRPIN803 and potassium carbonate to form alcohol **18** in a Williamson etherification reaction. Compound **18** was activated with 4-nitrophenyl chloroformate and triethylamine to yield the reactive carbamate **19**, which was subsequently reacted with oligopeptide c(RGDyK). Conjugate geo35 was purified by reversed-phase HPLC in 40% yield. The purity of geo35 was confirmed by LC-MS and was greater than 95%.

**In Vitro Stability Studies.** Chemostability Assay of geo41 and geo35. The stabilities of geo41 and geo35 conjugates in buffer, cell medium, and human plasma are presented below. Overall, the conjugates geo41 and geo35 were found to be stable at pH 7.4 and less stable at pH 5.2. After 5 h of incubation at pH 5.2, the residual concentration of geo41 represented 64% of the

### Scheme 3. Synthesis of SRPIN803 Derivatives Bearing a Carbamate Linker



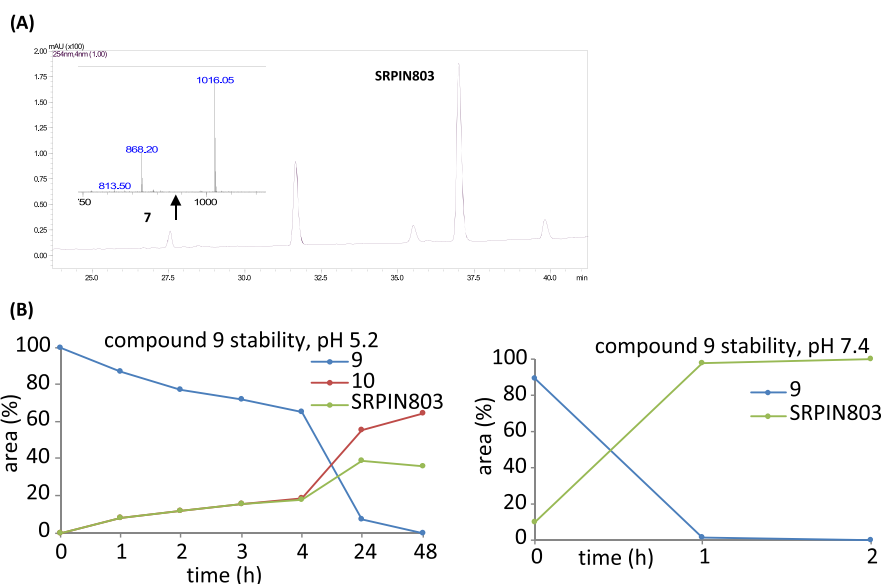
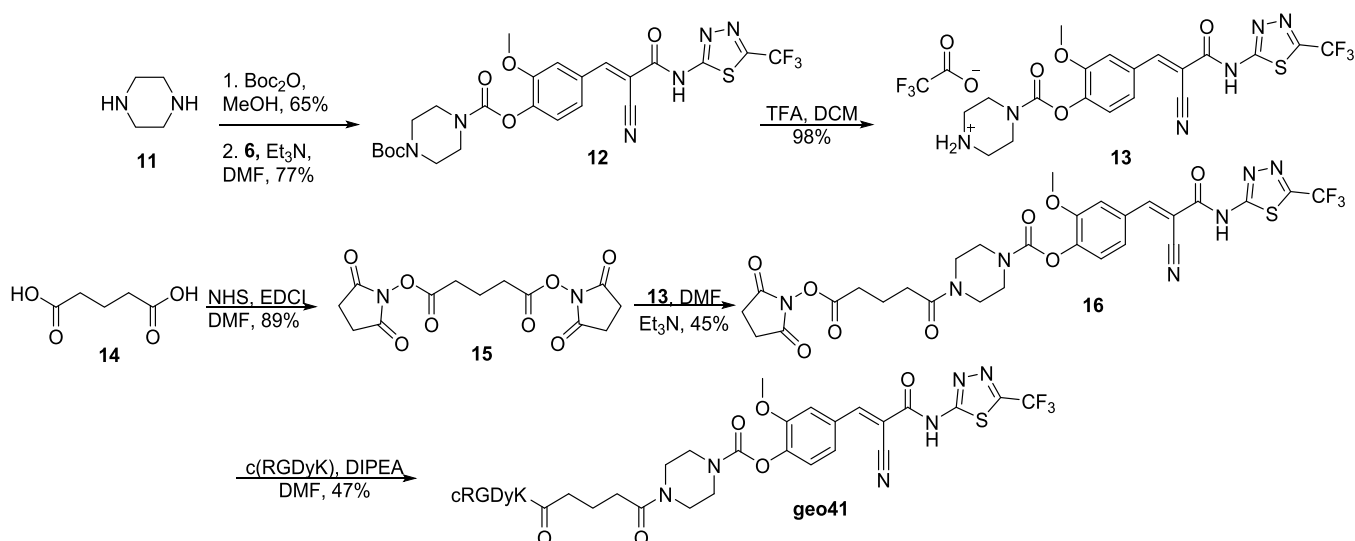
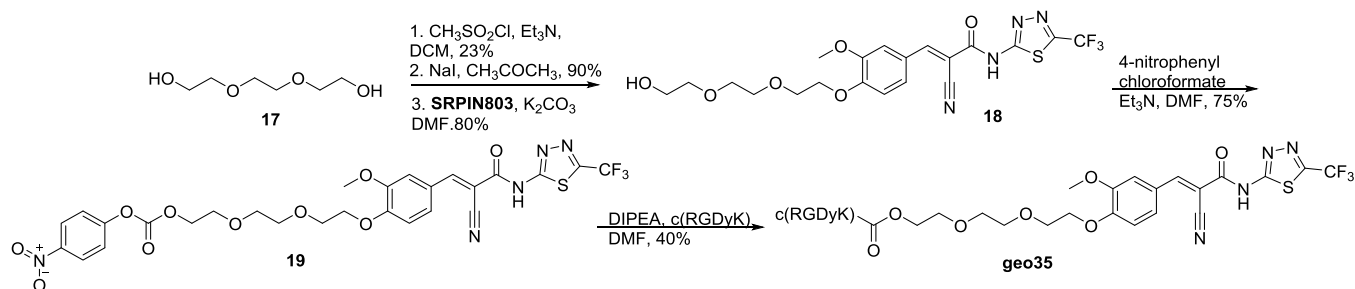


**Figure 3.** (A) LC/MS analysis of reaction mixture for the formation of 7. Compound 7 ESI-MS  $m/z$  for  $C_{42}H_{49}F_3N_{13}O_{12}S$  [ $M + H$ ] $^+$  calcd 1016.3296, found 1016.05. (B) Chemostability of 9 by LC-MS analysis. Results are presented as mean  $\pm$  SD for three independent experiments.

#### Scheme 4. Synthesis of SRPIN803-c(RGDyK) Conjugate Bearing a Secondary Carbamate Linker



#### Scheme 5. Synthesis of SRPIN803-c(RGDyK) Conjugate Bearing a Stable Ether Linker



initial concentration of geo41 (Figure 4). geo35 was more stable than geo41 at pH 5.2 and maintained more than 88% of its initial concentration. In acidic pH, geo41 and geo35 degraded with estimated half-lives of  $t_{1/2} = 13$  h 35 min and  $t_{1/2} = 43$  h 5 min, respectively. Notably, our studies show that the decomposition of both geo41 and geo35 is not associated with the stability of

the linkers toward hydrolysis and SRPIN803 release, but with a retro-Knoevenagel reaction and release of compound 2 (Scheme 6).

Having observed the retro-Knoevenagel decomposition of SRPIN803-c(RGDyK) conjugates, we tested whether SRPIN803 undergoes the same reaction. This finding would

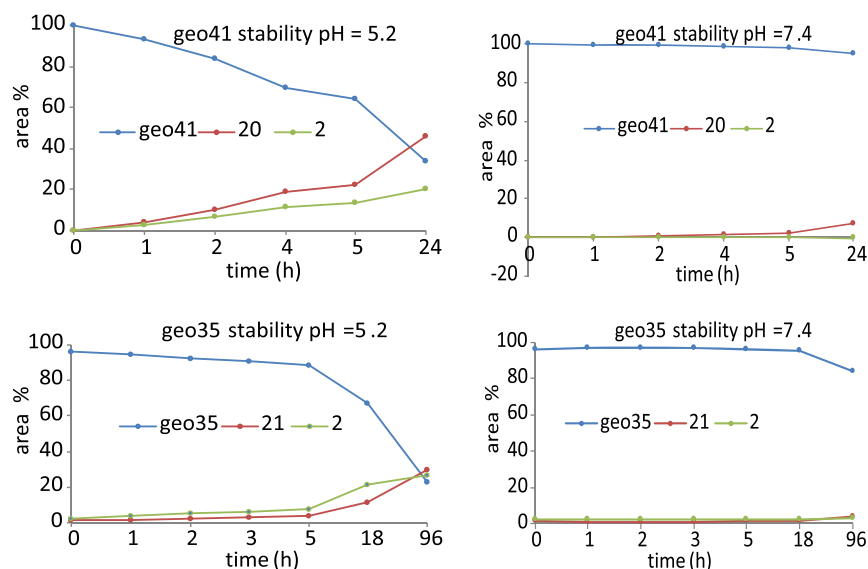


Figure 4. Chemostability of geo41 and geo35 by LC-MS analysis. Results are presented as mean  $\pm$  SD for three independent experiments.

#### Scheme 6. Retro-Knoevenagel Reactions of geo41 and geo35 after Incubation of the Conjugates at pH 5.2 and 7.4

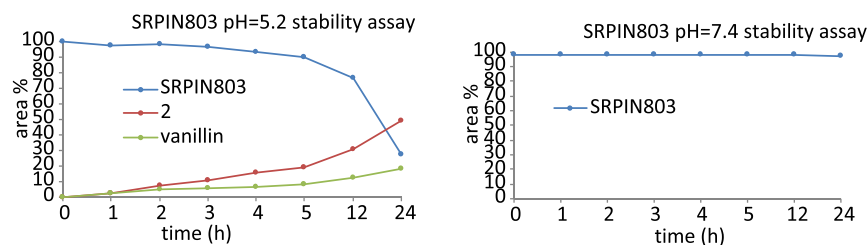
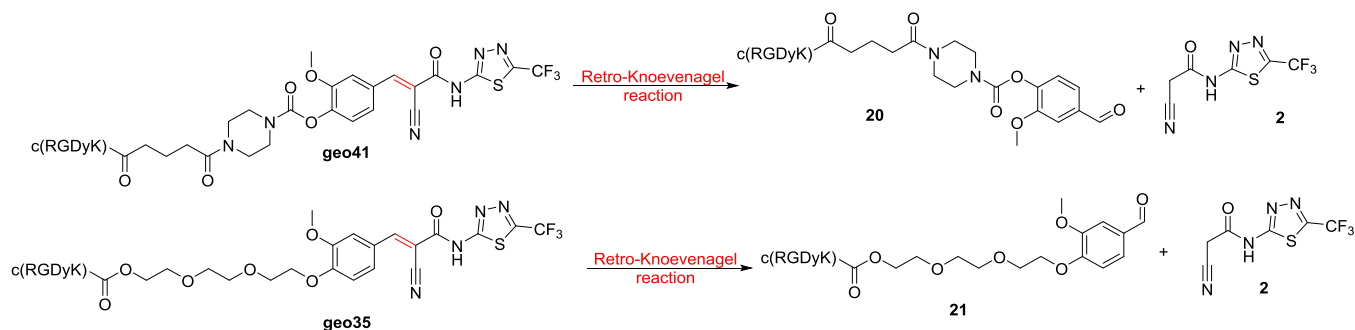


Figure 5. Chemostability of SRPIN803 by LC-MS analysis. Results are presented as mean  $\pm$  SD for three independent experiments.

be significant for further optimization studies, especially since SRPIN803 chemotype has been utilized as a lead compound for the development of potent and selective CK2 inhibitors targeting its open-hinge conformation.<sup>22</sup> SRPIN803 was stable at pH 7.4 and less stable at pH 5.2. In the second case, SRPIN803 released 2 and vanillin via the retro-Knoevenagel reaction and degraded slowly with estimated half-lives of 16 h and 30 min. After 12 h, SRPIN803 maintained more than 76% of its initial concentration (Figure 5).

**Biostability Assays of geo35 and geo41 in Dulbecco's Modified Eagle's Medium and Human Plasma.** The stability of geo35 and geo41 were also investigated in Dulbecco's modified Eagle's medium (DMEM) and human plasma. The stability was evaluated over 48 h in human plasma and DMEM and revealed the propensity of SRPIN803 conjugates to undergo a retro-Knoevenagel degradation (Figure 6). geo35 and geo41

displayed half-lives of  $t_{1/2} = 9$  h 6 min and  $t_{1/2} = 22$  h, respectively, in DMEM. Similar stabilities were recorded in human plasma where both conjugates maintained more than 67% of their initial concentration. geo35 had a half-life of  $t_{1/2} = 13$  h 54 min, and geo41 had a shorter half-life of  $t_{1/2} = 7$  h 50 min in human plasma.

**In Silico Studies and Biological Evaluation. Inhibition of Kinase Activity.** Our aim was to develop SRPIN803-c(RGDyK) hybrid compounds that would release SRPIN803 inside cells. Since the metabolism of these hybrid compounds is unknown, the inhibitory activity of SRPIN803 and SRPIN803-c(RGDyK) hybrid compounds against SRPK1 and CK2 was assessed by *in vitro* kinase assays. SRPIN803 inhibited the activity of SRPK1 toward LBRNt(62–92), a well-known substrate of the kinase,<sup>23</sup> with an  $IC_{50}$  value of 7.5  $\mu$ M, while the c(RGDyK)-conjugated compounds completely abolished its inhibitory activity (Table

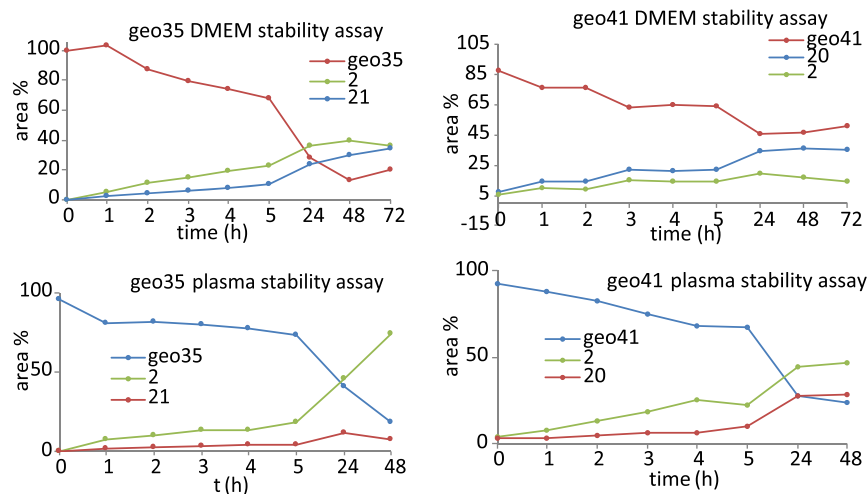


**Figure 6.** Biostability assays of geo41 and geo35 by LC-MS analysis. Results are presented as mean  $\pm$  SD for three independent experiments.

1). Confirming a previous report,<sup>13</sup> SRPIN803 inhibited more potently the activity of CK2 with an  $IC_{50}$  value of  $0.68 \mu M$ , while

**Table 1.** Half-Maximal Inhibitory Activity of SRPIN803, c(RGDyK), geo41, geo35, and 18 over SRPK1 and CK2 Kinases<sup>a</sup>

compound	$IC_{50}$ ( $\mu M$ )	
	CK2	SRPK1
SRPIN803	0.68	7.5
c(RGDyK)		
geo41	63.78	>100
geo35	85.21	>100
18	>200	>200

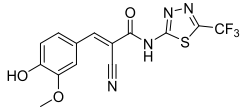
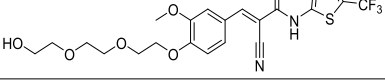
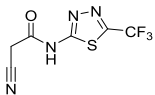
<sup>a</sup>The values are expressed as the means of three independent experiments.

the c(RGDyK)-conjugated compounds inhibited the kinase to a significantly lesser extent. The previously reported  $IC_{50}$  values for SRPIN803 were  $2.4 \mu M$  for SRPK1 and  $0.21 \mu M$  for CK2.<sup>13</sup> We have also tested the activity of intermediate compound 18,

which was found significantly less active from both SRPIN803 and the SRPIN803-c(RGDyK) conjugates.

**In Silico Studies of SRPIN803.** In a following step to better understand the interactions of SRPIN803 and its derivatives with SRPK1 and CK2 kinases, molecular docking studies were performed using the AutoDock Vina software.<sup>24</sup> Initially, the docking protocol was validated after removing the co-crystallized inhibitors and redocking them into the catalytic sites of SRPK1 (PDB ID: 4WUA) and CK2a (PDB ID: 6RB1) to determine the reliability of the applied docking protocol (Supporting Information Figure S56). Table 2 presents the binding energy of docked SRPIN803 and its derivatives into the catalytic sites of SRPK1 and CK2a, respectively. Docking analysis shows that SRPIN803 has a binding energy equal to  $-9.4$  kcal/mol for SRPK1 and  $-10.5$  kcal/mol for CK2. A closer look at the interactions between SRPIN803 and SRPK1 (Figure 7) revealed that the phenol moiety was bound via a hydrogen bond to Glu124 ( $3.01 \text{ \AA}$ ), while the carbonyl oxygen of the amide behaves as a hydrogen-bond acceptor and the NH group of Leu168 ( $3.05 \text{ \AA}$ ). This specific hydrogen-bonding network enabled SRPIN803 to form additional van der Waals, pi-pi

**Table 2.** Binding Energy of Docked SRPIN803, geo33, and 2 into the Catalytic Sites of SRPK1 (PDB ID: 4WUA) and CK2a (PDB ID: 6RB1)

Compound	Binding Energy for SRPK1 kcal/mol	Binding Energy for CK2 kcal/mol
SRPIN803 	-9.4	-10.5
geo33 	-8.2	-8.3
2 	-6.9	-7.1

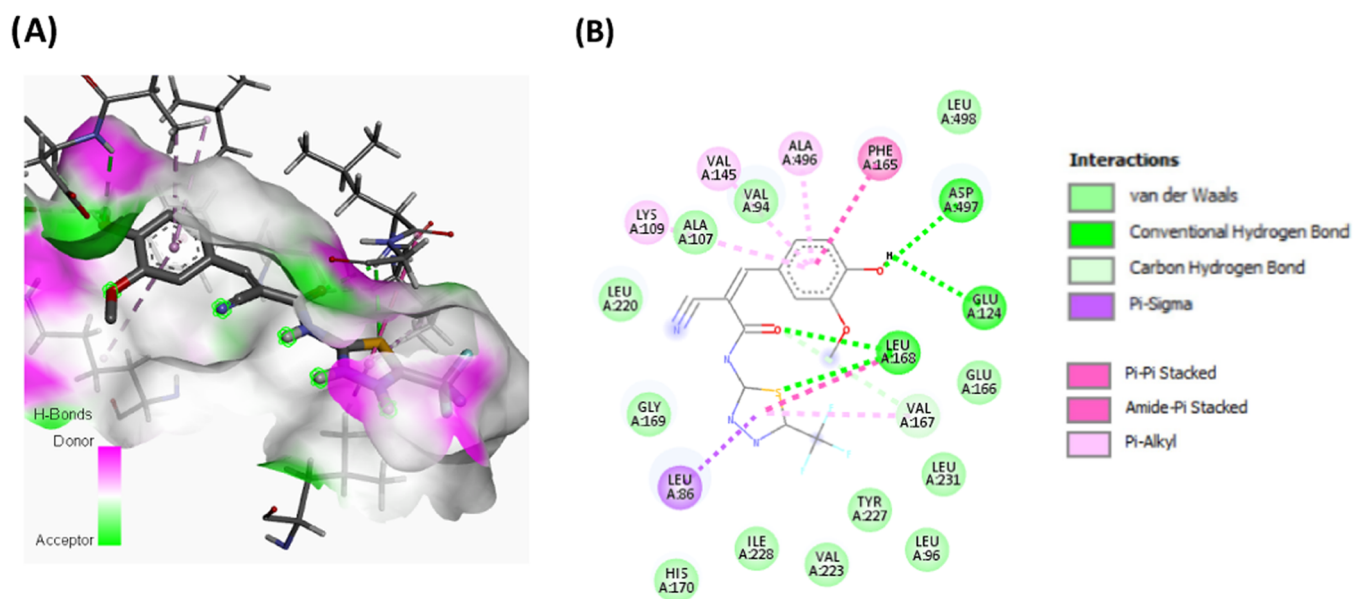


**Figure 7.** (A) Docking pose of SRPIN803 in SRPK1 binding site. (B) 2D plot of interactions between SRPIN803 and key residues of SRPK1 generated by BIOVIA Discovery Studio visualizer. Molecular interactions—hydrogen and hydrophobic bonds are indicated by green and pink/purple dashed lines.

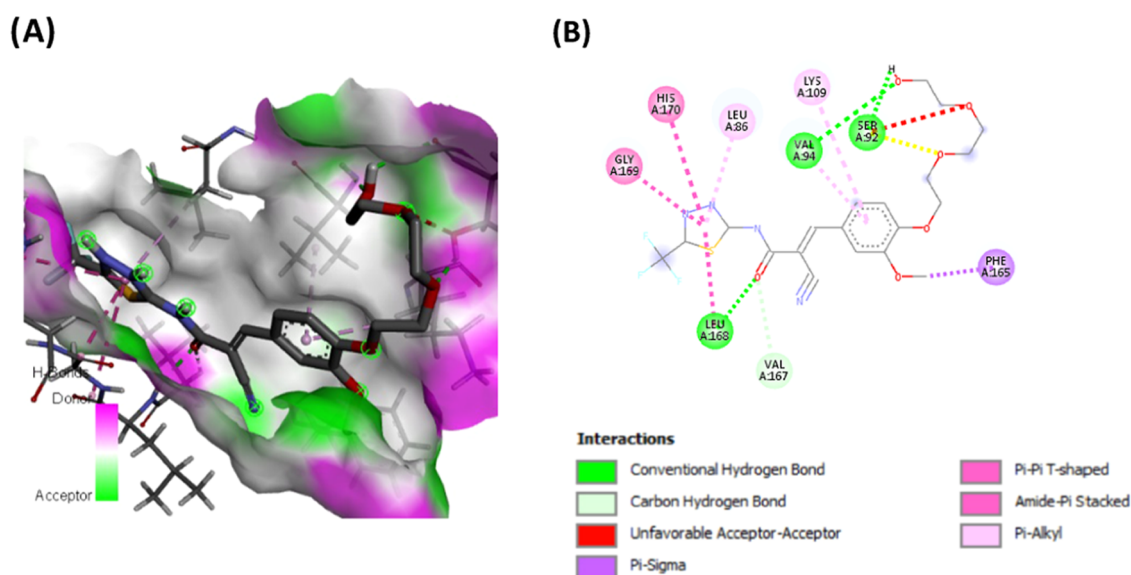


**Figure 8.** (A) Docking pose of geo33 in SRPK1 binding site. (B) 2D plot of interactions between geo33 and key residues of SRPK1 generated by BIOVIA Discovery Studio visualizer. Molecular interactions—hydrogen, hydrophobic bonds and unfavorable acceptor–acceptor are indicated by green, pink/purple and red dashed lines.

stacking, pi–amide, pi–alkyl, and pi–sigma interactions with neighboring residues. In the case of geo33, the binding energy was lower for both kinases. Analysis of the best-ranked docking pose of geo33 into SRPK1 shows two strong hydrogen bonds with Ser92 (2.33 Å) and Leu168 (2.15 Å) and several hydrophobic interactions (Figure 8). However, geo33 has an unfavorable acceptor–acceptor interaction with Ser92, which indicates the repulsion between Ser92 and the oxygen of the ethylene glycol linker. Docking analysis of **2** shows two hydrogen bonds with His170 (3.06 Å) and Leu168 (2.29 Å), several hydrophobic interactions and a fluorine carbonyl group of Glu166. The binding of **2** into the catalytic sites of SRPK1 is weaker in comparison with SRPIN803 (Figure 9).

Molecular docking of SRPIN803 and its derivatives against CK2 was also carried out to predict the affinity of these compounds (Figures S57 and S58). All compounds displayed better binding energies for CK2 (Table 2). As a general outcome, the docking results for SRPIN803 are consistent with the measured *in vitro* kinase activity of the compound against SRPK1 ( $IC_{50} = 2.4 \mu M$ ) and CK2 ( $IC_{50} = 0.21 \mu M$ ). Derivative geo33 that could be released from the conjugate geo35 and **2** that could be derived from both geo35 and geo41 *in vivo* after the Knoevenagel degradation were both found less active in docking and *in vitro* kinase experiments.

**Cytotoxicity of SRPIN803-c(RGDyK) Conjugates.** The cytotoxic activity of SRPIN803 and SRPIN803-c(RGDyK) hybrids was evaluated at different concentrations (10–100  $\mu M$ )

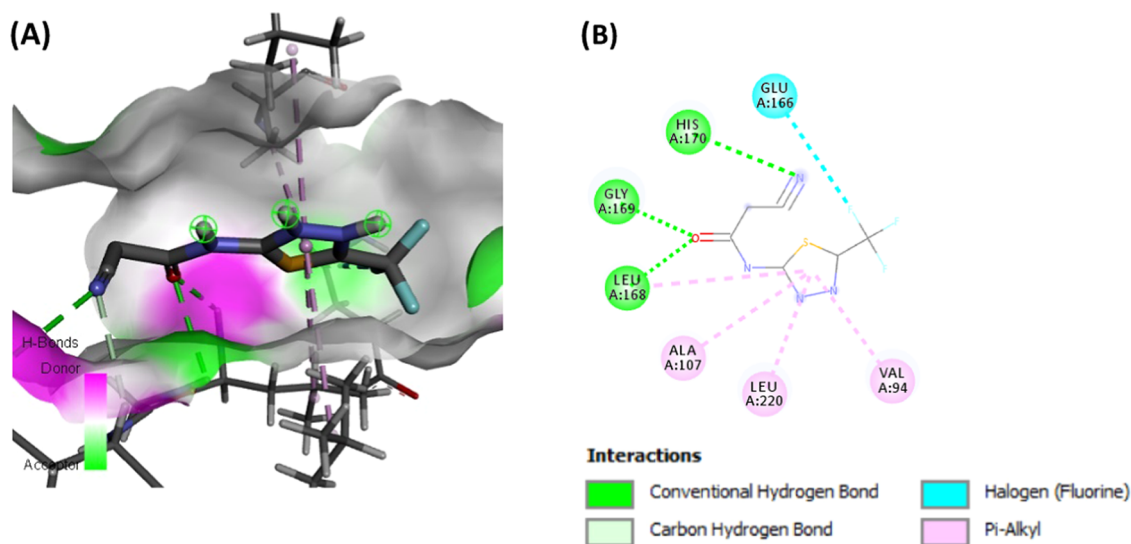


**Figure 9.** (A) Docking pose of 2 in SRPK1 binding site. (B) 2D plot of interactions between 2 and key residues of SRPK1 generated by BIOVIA Discovery Studio visualizer. Molecular interactions—hydrogen and hydrophobic bonds and halogen are indicated by green, pink/purple, and light blue dashed lines, respectively.

**Table 3. Growth Inhibition/Cytostatic ( $GI_{50}$  and TGI) and Cytotoxic/Cytocidal ( $IC_{50}$ ) Anticancer Effects Induced by SRPIN803, c(RGDyK), and SRPIN803-c(RGDyK) Hybrid Compounds against a Panel of Cancer Cell Lines**

	SRPIN803			geo41			geo35			c(RGDyK)		
	$GI_{50}$ ( $\mu M$ )	TGI ( $\mu M$ )	$IC_{50}$ ( $\mu M$ )	$GI_{50}$ ( $\mu M$ )	TGI ( $\mu M$ )	$IC_{50}$ ( $\mu M$ )	$GI_{50}$ ( $\mu M$ )	TGI ( $\mu M$ )	$IC_{50}$ ( $\mu M$ )	$GI_{50}$ ( $\mu M$ )	TGI ( $\mu M$ )	$IC_{50}$ ( $\mu M$ )
A549	>100	>100	>100	$32 \pm 0.5$	$84 \pm 0.9$	>100	$10 \pm 1.6$	$44 \pm 2.8$	$83 \pm 3.2$	$61 \pm 9$	>100	>100
MCF7	>100	>100	>100	$50 \pm 1.4$	>100	>100	$12 \pm 0.5$	$21 \pm 0.9$	$61 \pm 1.4$	>100	>100	>100
Hcc827	$88 \pm 2.2$	>100	>100	$76 \pm 2.5$	>100	>100	$13 \pm 1.1$	$64 \pm 1.5$	>100			
MRC5	>100	>100	>100	$49 \pm 1.5$	>100	>100	$16 \pm 0.5$	$32 \pm 1.0$	$63 \pm 1.8$			
PC3	$80 \pm 0.8$	>100	>100	$60 \pm 1.8$	>100	>100	$10 \pm 0.8$	$33 \pm 1.1$	$92 \pm 1.9$	$74.4 \pm 7$	>100	>100
HeLa	>100	>100	>100	$72 \pm 1.9$	>100	>100	$81 \pm 1.7$	>100	>100	$79 \pm 2.2$	>100	>100
U87	$94 \pm 0.4$	>100	>100	$63 \pm 0.9$	>100	$78 \pm 1.3$	$61 \pm 1.1$	>100	$75 \pm 2.3$	$63 \pm 2.5$	>100	$77 \pm 3.7$

over a panel of cell lines including lung cancer cells A549, mammary carcinoma cells MCF7, lung adenocarcinoma cells Hcc827, normal human fetal lung fibroblasts MRC5, prostate cancer cells PC3, cervical cancer cells HeLa, and glioblastoma cells U87. The cytostatic and cytotoxic activities of the SRPIN803-c(RGDyK) hybrid compounds were measured by three concentration-dependent parameters:  $GI_{50}$  (concentration that produces 50% growth inhibition), TGI (concentration that produces total growth inhibition or cytostatic effect), and  $IC_{50}$  (concentration that produces  $-50\%$  growth, cytotoxic effect) and are presented in Table 3.

SRPIN803 was demonstrated to be slightly cytostatic against Hcc827, PC3, and U87 ( $GI_{50} = 80\text{--}98 \mu M$ ). A similar activity against A549, PC3, HeLa, and U87 cancer cells was recorded for c(RGDyK) ( $GI_{50} = 61\text{--}79 \mu M$ ), which also displayed a minor cytotoxicity against glioblastoma cells U87 ( $IC_{50} = 77 \mu M$ ). Derivative geo41 bearing a cleavable carbamate linker inhibited the growth of all tested cell lines ( $GI_{50} = 32\text{--}76 \mu M$ ). The most active compound in this study was geo35. The  $GI_{50}$  values significantly differed displaying a range of responses in A549, Hcc827, and PC3 ( $GI_{50} = 10\text{--}16 \mu M$ , TGI =  $21\text{--}44 \mu M$ ). For the most sensitive cell lines MCF7 and MRC5, the  $IC_{50}$  values were 61 and  $63 \mu M$ , respectively. These results clearly provide evidence that the conjugation of SRPIN803 to c(RGDyK) peptide is beneficial for anticancer activity; however, the

compounds possess only moderate activities against the tested cell lines and were also toxic against MRC5 lung normal cells.

**SRPIN803 and SRPIN803-c(RGDyK) Conjugates Effect on Zebrafish Angiogenesis.** To determine if SRPIN803 and SRPIN803-c(RGDyK) conjugates have any effect on angiogenesis, embryos from the transgenic zebrafish line *Tg(kdrl:gfp)* have been employed. We added the compounds in the embryo water 24 h post fertilization (hpf) and scored angiogenesis in the intersegmental vessels (ISVs) at 72hpf. The embryos were examined under a fluorescence microscope, and the length of the ISVs was used as a measurement to evaluate angiogenesis. Our study indicated that SRPIN803 could inhibit zebrafish angiogenesis without any additional morphological phenotype (Figure 10).

To determine whether the conjugated compounds did not significantly inhibit angiogenesis due to their kinetics and diffusion properties in the embryo water, we additionally injected them in the developing embryo at the one-cell stage. We measured ISV length as in Figure 11 at 72hpf. Our results show that both SRPIN803 and geo35 could inhibit zebrafish angiogenesis, with geo35 exhibiting a milder effect than SRPIN803, while the other two compounds tested did not show a significant inhibition.



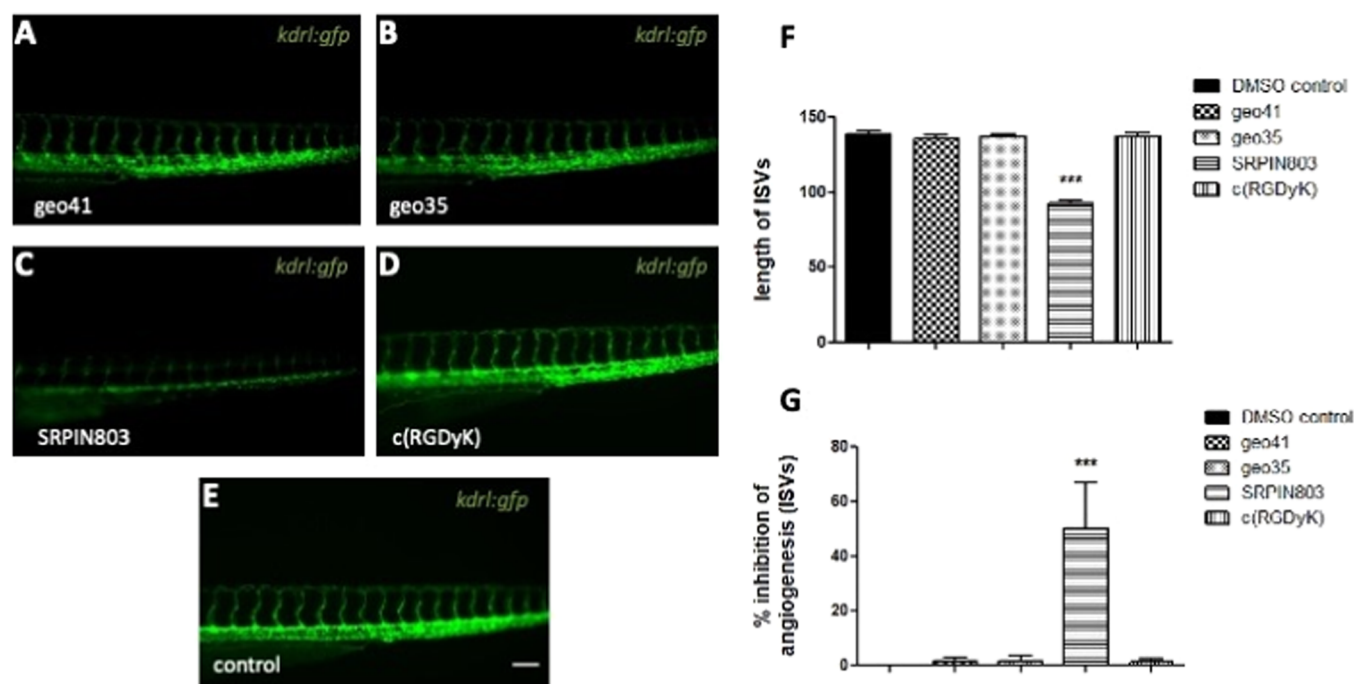


**Figure 10.** *In vivo* screening reveals SRPIN803 as a master inhibitor of angiogenesis upon zebrafish treatment assay. (A–E) Fluorescence microscopy images of representative compound treated from 24hpf, and DMSO-treated control 72hpf *Tg(kdr1:gfp)* embryos. Scale bar, 100  $\mu$ m. (F) The total length of 10 ISVs per embryo was measured and presented. SRPIN803 shows statistically significant inhibition of ISVs, while the other tested compounds had no effect at the tested concentration. (G) The percentage of inhibition of angiogenesis was calculated compared to DMSO-treated controls for each compound. Data are expressed as mean + SEM ( $n = 20$ /group).  $p^{***} < 0.001$ .

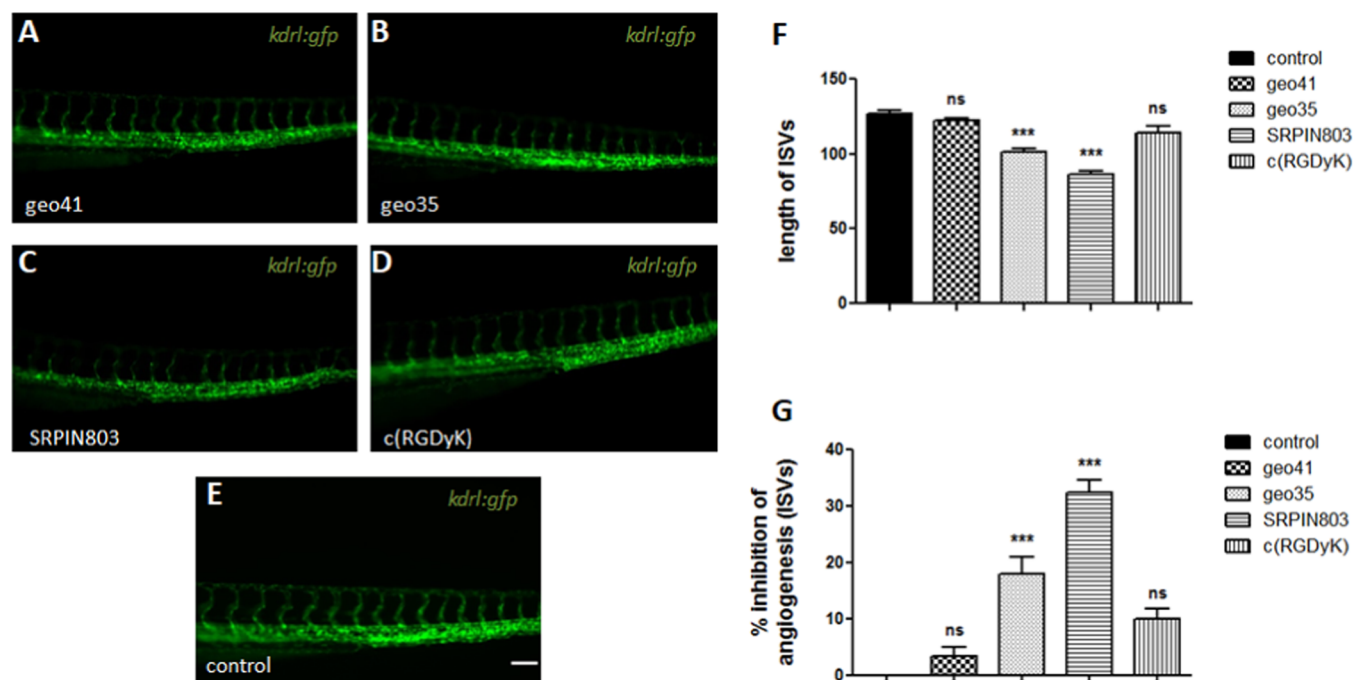


**Figure 11.** *In vivo* zebrafish screening unravels two inhibitors of angiogenesis. (A–D) Fluorescence microscopy images of representative injected and uninjected control (E) at 72hpf of *Tg(kdr1:gfp)* embryos. Scale bar, 100  $\mu$ m. (F) The total length of 10 ISVs per embryo was measured and presented. Both geo35 and SRPIN803 block angiogenesis, with geo35 exhibiting a milder effect than SRPIN803. (G) The percentage of the inhibition of angiogenesis was calculated compared to uninjected sibling controls for each compound. Data are expressed as mean + SEM ( $n = 30$ /group).  $p^{***} < 0.001$ .

## DISCUSSION

In the current study, to develop new antiangiogenic agents based on SRPIN803, we have designed and synthesized SRPIN803-c(RGDyK) hybrid compounds and studied their antiprolifer-

ative and antiangiogenic properties. These hybrid compounds are formed by coupling of SRPIN803 with the c(RGDyK) pentapeptide; both are reported to have antiangiogenic properties affecting distinct pathways. SRPIN803 acts by

inhibiting both SRPK1 and CK2 kinases, while c(RGDyK) binds to  $\alpha_v\beta_3$  and  $\alpha_v\beta_5$  integrins.

Stability studies of the new hybrids showed sufficient stability profiles; however, detailed analysis revealed that they did not release SRPIN803 but the fragments geo33 and 2 from a retro-Knoevenagel reaction. In our study, SRPIN803 inhibited SRPK1 with an  $IC_{50}$  value of 7.5  $\mu\text{M}$  and CK2 with an  $IC_{50}$  of 0.68  $\mu\text{M}$ , while the synthesized conjugates inhibited both kinases to a significantly lesser extent ( $IC_{50}$  value > 63  $\mu\text{M}$ ). To shed light to the observed activities, molecular docking of SRPIN803 and its derivatives against the two kinases was performed. The docking results agree with the measured *in vitro* kinase activity of SRPIN803, geo33, and 2. Fragment 2 that could be derived from both geo35 and geo41 *in vivo* after the Knoevenagel reaction and was found significantly less active than SRPIN803 with docking scores of -6.9 and -7.1 kcal/mol against SRPK1 and CK2 kinases, respectively.

The *In vitro* properties of conjugates geo35 and geo41 were also evaluated against a panel of cancer cells by the MTT method. SRPIN803 and c(RGDyK) were demonstrated to be slightly cytostatic on cell lines used to study, while both conjugates were found more active. The most potent compound was geo35 that was cytostatic in A549, Hcc827, and PC3 ( $GI_{50}$  = 10–16  $\mu\text{M}$ , TGI = 21–44  $\mu\text{M}$ ) and cytotoxic for the most sensitive cell lines MCF7 and MRC5 with  $IC_{50}$  values of 61 and 63  $\mu\text{M}$ , respectively. These findings clearly indicate that the conjugation of SRPIN803 to c(RGDyK) peptide is beneficial for cytotoxic impact against A549, MCF7, PC3, and U87 cancer cells, but the hybrids are not selective against cancer cells but affect the normal MRC5 cells.

We have further investigated the potential of the SRPIN803 and SRPIN803-c(RGDyK) conjugates to affect angiogenesis, using the transgenic zebrafish line *Tg(kdrl:gfp)* embryos. Our data suggest that SRPIN803 is active in both experimental setups we used. We found that geo35 in an aqueous environment is not able to act through diffusion to inhibit *in vivo* zebrafish angiogenesis. However, when injected in the embryo, geo35 showed significant inhibitory activity.

## CONCLUSIONS

Recent studies show that the combination of antiangiogenic sunitinib with an  $\alpha_v\beta_3$  integrin antagonist cRGDfK peptide displays a synergistic anticancer effect in human lung adenocarcinoma cells.<sup>25</sup> In the present study, SRPIN803 and geo35 were identified to hold antiangiogenic activity *in vivo* in zebrafish embryos, and this effect was dose-dependent. Although the c(RGDyK)-SRPIN803 hybrid compounds were found less potent compared to SRPIN803, they have shown activities interesting enough to illustrate the potential of this approach for the development of a new class of antiangiogenic compounds.

## EXPERIMENTAL PROCEDURES

**General Experimental Details.** All reactions were carried out under an atmosphere of Ar. The reagents were purchased and used without further purification. Reactions were monitored by TLC and using UV light as a visualizing agent and aqueous ceric sulfate/phosphomolybdic acid, ethanolic *p*-anisaldehyde solution, potassium permanganate solution, and heat as developing agents.  $^1\text{H}$  and  $^{13}\text{C}$  NMR spectra were recorded at 500 and 125 MHz (Agilent) with tetramethylsilane as an internal standard. Chemical shifts are indicated in  $\delta$  values

(ppm) from internal reference peaks (TMS  $^1\text{H}$  0.00;  $\text{CDCl}_3$   $^1\text{H}$  7.26,  $^{13}\text{C}$  77.00,  $\text{CD}_3\text{OD}$   $^1\text{H}$  3.30,  $^{13}\text{C}$  49.00). LC-MS spectra were recorded on an LC-20AD Shimadzu device connected to a Shimadzu LCMS-2010EV equipped with a C18 analytical column (Supelco Discovery C18, 5  $\mu\text{m}$  250  $\times$  4.6 mm). IR spectra were recorded in model FTIR-2000 (PerkinElmer, Waltham, MA). Potassium bromide was used for the formation of suitable disks before the analysis. All spectra were collected from 400 to 4000  $\text{cm}^{-1}$  with 4  $\text{cm}^{-1}$  resolution (10 co-added scans), and the baseline was corrected and converted into transmittance mode. Infusion experiments were carried out on an Agilent Q-TOF mass spectrometer, G6540B, a model with Dual AJS ESI-MS. All of the compounds (dissolved in LC-MS-grade methanol or ACN/ $\text{H}_2\text{O}$ ) were introduced into the ESI source of the MS with a single injection of 15  $\mu\text{L}$  of the sample and with a flow rate of 300  $\mu\text{L}/\text{min}$  of 100% methanol as a solvent in the binary pump. The experiments were run using a Dual AJS ESI source, operating in a positive ionization mode. Source operating conditions were 330  $^\circ\text{C}$  gas temperature, 8 L/min gas flow, 250  $^\circ\text{C}$  sheath gas temperature, 10 L/min sheath gas flow, and 50–100 V fragmentor. All accurate mass measurements of the  $[\text{M} + \text{H}]^+$  or  $[\text{M} + \text{Na}]^+$  ions were achieved at a mass rate of 50–1000  $m/z$  in positive mode. The Q-TOF was calibrated 1 h prior to the infusion experiments using a calibration mixture. Data were acquired in an external calibration mode.

(*E*)-2-Cyano-3-(4-hydroxy-3-methoxyphenyl)-*N*-(5-(trifluoromethyl)-1,3,4-thiadiazol-2-yl)acrylamide, **SRPIN803**. Methyl cyanoacetate (0.26 mL, 2.927 mmol) and sodium methoxide (319 mg, 5.913 mmol) were added to a solution of 2-amino-5-trifluoromethyl-1,3,4-thiadiazole **1** (500 mg, 2.956 mmol) in methanol (8.8 mL) at room temperature under an argon atmosphere. After stirring for 20 h at 60  $^\circ\text{C}$ , the mixture was concentrated under reduced pressure to give a yellow solid. Under an argon atmosphere, acetonitrile (7.9 mL), vanillin (211.7 mg, 1.391 mmol), ammonium acetate (100 mg, 1.349 mmol), and acetic acid (64  $\mu\text{L}$ , 1.099 mmol) were added to a part of the solid (390 mg). After stirring for 1 h at 90  $^\circ\text{C}$ , the solvent was removed under reduced pressure and the residue was purified by silica gel column chromatography (eluent; DCM/MeOH 100/2 to 100/15) to give **SRPIN803** (370 mg, 67%) as a yellow solid. The spectral data were in accordance with those reported in the literature.<sup>13</sup> **SRPIN803**:  $^1\text{H}$  NMR (500 MHz,  $\text{DMSO}-d_6$ )  $\delta$  10.60 (s, 1H), 8.45 (s, 1H), 7.73 (s, 1H), 7.54 (d,  $J$  = 8.4 Hz, 1H), 6.98 (d,  $J$  = 8.3 Hz, 1H), 3.83 (s, 3H);  $^{13}\text{C}$  NMR (126 MHz,  $\text{DMSO}-d_6$ )  $\delta$  163.5, 163.1, 153.5, 152.9, 150.7, 147.9, 127.6, 122.8, 119.8, 116.5, 116.6, 113.4, 99.5, 55.5; ESI-MS, negative mode:  $m/z$  calcd mass for  $\text{C}_{14}\text{H}_9\text{F}_3\text{N}_4\text{O}_3\text{S}$   $[\text{M} - \text{H}]^-$  = 369.03, was found 368.75.

2-((2-((*tert*-Butyldimethylsilyloxy)ethyl)disulfanyl)ethan-1-ol, **S1**. 2,2'-Dithiodiethanol (100 mg, 0.648 mmol) was dissolved in dry DCM (4 mL), and a solution of imidazole (44 mg, 0.648 mmol) in anhydrous DMF (0.1 mL) was added. Next, a solution of *tert*-butyldimethylsilyl chloride (98 mg, 0.648 mmol) in dry DCM (0.5 mL) was added and the reaction mixture was stirred at room temperature for 18 h. Subsequently, imidazole (66 mg, 0.972 mmol) and *tert*-butyldimethylsilyl chloride (147 mg, 0.972 mmol) were added and the mixture was stirred for another 18 h. The solvent was removed under reduced pressure and the mixture was extracted with EtOAc. The organic extracts were dried over  $\text{Na}_2\text{SO}_4$  and concentrated to dryness under reduced pressure. The residue was purified by silica gel column chromatography (eluent: hexane/EtOAc = 8/

1) to give **S1** (58 mg, 33% yield) as a colorless liquid. The spectral data were in accordance with those reported in the literature.<sup>26</sup> **S1**: <sup>1</sup>H NMR (500 MHz, CDCl<sub>3</sub>) δ 3.88 (t, *J* = 5.8 Hz, 2H), 3.86 (7, *J* = 5.8 Hz, 2H), 2.85 (t, *J* = 5.0 Hz, 2H), 2.83 (t, *J* = 5.8 Hz, 2H), 0.89 (s, 9H), 0.07 (s, 6H); <sup>13</sup>C NMR (126 MHz, CDCl<sub>3</sub>) δ 61.8, 60.2, 41.3, 41.2, 25.8, 18.3, -5.3.

2-((2-((*tert*-Butyldimethylsilyloxy)ethyl)disulfanyl)ethyl (4-nitrophenyl) carbonate, **S2**. 4-Nitrophenyl chloroformate (90 mg, 0.45 mmol) was added to a stirred solution of **S1** (100 mg, 0.37 mmol) in dry DCM (1.2 mL) and triethylamine (0.16 mL, 1.12 mmol) at 0 °C under argon. As the solution turned yellow, the mixture was stirred at room temperature for 3 h. The solvent was removed under reduced pressure, and the residue was purified by silica gel chromatography (eluent: hexane/EtOAc = 20/1 to 5/1) to afford **S2** (136 mg, 84% yield) as a sub-yellow oil. **S2**: <sup>1</sup>H NMR (500 MHz, CDCl<sub>3</sub>) δ 8.36–8.18 (m, 2H), 7.39 (d, *J* = 9.2 Hz, 2H), 4.55 (t, *J* = 6.6 Hz, 2H), 3.87 (t, *J* = 6.6 Hz, 2H), 3.02 (t, *J* = 6.6 Hz, 2H), 2.87 (t, *J* = 6.6 Hz, 2H), 0.90 (s, 9H), 0.08 (s, 6H). <sup>13</sup>C NMR (126 MHz, CDCl<sub>3</sub>) δ 155.4, 152.3, 145.4, 125.3, 121.7, 66.9, 61.7, 41.6, 36.6, 25.9, 18.3, -5.3.

(*E*)-2-((2-((*tert*-Butyldimethylsilyloxy)ethyl)disulfanyl)ethyl (4-(2-cyano-3-oxo-3-((5-(trifluoromethyl)-1,3,4-thiadiazol-2-yl)amino)prop-1-en-1-yl)-2-methoxyphenyl) carbonate, **5**. Triethylamine (35 μL, 0.254 mmol) was added to a stirred solution of SRPIN803 (47 mg, 0.127 mmol) and **S2** (55 mg, 0.127 mmol) in dry DMF (2.1 mL) under argon, and the mixture was stirred at room temperature for 2 days. The solvent was removed under reduced pressure, and the residue was purified by silica gel chromatography (eluent: hexane/EtOAc = 5/1 to 1/2) eluted **5** (65.8 mg, 78% yield) as a yellow solid. **5**: <sup>1</sup>H NMR (500 MHz, CDCl<sub>3</sub>) δ 8.46 (s, 1H), 7.85 (s, 1H), 7.55 (d, *J* = 8.3 Hz, 1H), 7.32 (d, *J* = 8.3 Hz, 1H), 4.54 (t, *J* = 6.6 Hz, 2H), 3.95 (s, 3H), 3.87 (t, *J* = 6.4 Hz, 2H), 3.02 (t, *J* = 6.6 Hz, 2H), 2.86 (t, *J* = 6.5 Hz, 2H), 0.90 (s, 9H), 0.08 (s, 6H). <sup>13</sup>C NMR (126 MHz, CDCl<sub>3</sub>) δ 161.5, 159.8, 155.3, 153.5, 152.1, 151.9, 144.6, 129.9, 126.5, 123.3, 119.5, 115.4, 113.4, 101.8, 66.9, 61.7, 56.3, 41.6, 36.6, 25.9, 18.3, -5.3; ESI-HRMS, negative mode: *m/z* calcd mass for C<sub>25</sub>H<sub>31</sub>F<sub>3</sub>N<sub>4</sub>O<sub>6</sub>S<sub>3</sub>Si [M - H]<sup>-</sup> = 663.1054, was found 663.0937.

*tert*-Butyl (2-(2-(2-aminoethoxy)ethoxy)ethyl)carbamate, **8**. The diamine (450 mg, 3 mmol) in dry DCM solution (10 mL/1 mmol) was treated with Boc<sub>2</sub>O (0.1 mL, 0.46 mmol) for 5 h at 0 °C and for 18 h at room temperature. The organic phase was washed with water until all of the unreacted diamine was extracted, dried over Na<sub>2</sub>SO<sub>4</sub>, filtered, and concentrated under reduced pressure. The residue was purified by column chromatography (eluent: DCM/MeOH = 9/1 to 4/1) to afford **8** as a colorless oil (110 mg, 97%). The spectral data were in accordance with those reported in the literature.<sup>27</sup>

(*E*)-*tert*-Butyl (4-(2-cyano-3-oxo-3-((5-(trifluoromethyl)-1,3,4-thiadiazol-2-yl)amino)prop-1-en-1-yl)-2-methoxyphenyl) ((ethane-1,2-diylbis(oxy))bis(ethane-2,1-diyl))dicarbamate, **9**. 4-Nitrophenyl chloroformate (8.1 mg, 0.041 mmol) was added to a stirred solution of SRPIN803 (10 mg, 0.027 mmol) in dry DMF (0.5 mL) and triethylamine (15 μL, 0.108 mmol) at 0 °C under argon. The mixture was stirred at room temperature, and after 2.5 h, **8** (6.7 mg, 0.027 mmol) in DMF (0.2 mL) and triethylamine (5.6 μL, 0.041 mmol) were added and the reaction was stirred at room temperature overnight. The solvent was removed under reduced pressure, and the residue was purified by column chromatography (eluent: DCM/acetone = 4/1) to give **9** (11 mg, 63% yield)

as a yellow solid. **9**: <sup>1</sup>H NMR (500 MHz, acetone-*d*<sub>6</sub>) δ 8.58 (s, 1H), 7.92 (s, 1H), 7.71 (d, *J* = 8.3 Hz, 1H), 7.35 (d, *J* = 8.3 Hz, 1H), 6.95 (s, 1H), 5.89 (s, 1H), 3.93 (s, 3H), 3.63 (m, 6H), 3.54 (t, *J* = 5.7 Hz, 2H), 3.40 (dd, *J* = 5.6 Hz, 2H), 3.25 (dd, *J* = 11.2, 5.6 Hz, 2H), 1.40 (s, 9H), <sup>13</sup>C NMR (126 MHz, acetone-*d*<sub>6</sub>) δ 162.8, 162.5, 156.1, 153.5, 153.3, 152.4, 151.2, 144.9, 129.7, 124.8, 124.1, 120.2, 115.3, 114.1, 104.2, 77.7, 70.2, 70.0, 69.8, 69.4, 55.6, 41.1, 40.2, 27.7; ESI-MS, negative mode: *m/z* calcd mass for C<sub>26</sub>H<sub>30</sub>F<sub>3</sub>N<sub>6</sub>O<sub>8</sub>S [M - H]<sup>-</sup> = 643.18, was found 642.90.

*tert*-Butyl piperazine-1-carboxylate, **S3**. A solution of di-*tert*-butyl dicarbonate (200 mg, 2.32 mmol) in dry methanol (4 mL) was added dropwise to piperazine (0.172 g, 2 mmol) in dry methanol (8.8 mL) during 30' with stirring, at 0 °C, under argon. The reaction mixture was stirred for 2 h, then the methanol was evaporated, and the residue was extracted three times with ethyl acetate. The combined extracts were dried over Na<sub>2</sub>SO<sub>4</sub> and concentrated under reduced pressure. Column chromatography of the crude product over silica gel (eluent: DCM/MeOH = 10/0.2 to 10/2) afforded the desired Boc derivative **S3** as a colorless solid (140 mg, 65%). The spectral data were in accordance with those reported in the literature.<sup>28</sup> **S3**: <sup>1</sup>H NMR (500 MHz, CDCl<sub>3</sub>) δ 3.45–3.36 (m, 4H), 2.87–2.77 (m, 4H), 1.46 (s, 9H).

(*E*)-1-*tert*-Butyl 4-(4-(2-cyano-3-oxo-3-((5-(trifluoromethyl)-1,3,4-thiadiazol-2-yl)amino)prop-1-en-1-yl)-2-methoxyphenyl) piperazine-1,4-dicarboxylate, **12**. 4-Nitrophenyl chloroformate (22.9 mg, 0.113 mmol) was added to a stirred solution of SRPIN803 (30 mg, 0.081 mmol) in dry DMF (2.10 mL) and triethylamine (25 μL) at 0 °C under argon. As the solution turned orange, the mixture was stirred at room temperature and monitored by TLC. After 3 h, **S3** (15 mg, 81 μmol) and triethylamine (11 μL) were added, and the reaction was stirred at room temperature overnight. The solvent was removed under vacuum, and the residue was chromatographed on silica gel (eluent: DCM/acetone = 4/0.1 to 4/1 and then DCM/MeOH = 10/0.5 to 10/2) to give **12** (36.5 mg, 77% yield) as a yellow white solid. **12**: <sup>1</sup>H NMR (500 MHz, CDCl<sub>3</sub>) δ 8.42 (s, 1H), 7.81 (s, 1H), 7.51 (d, *J* = 8.3 Hz, 1H), 7.26 (2H overlapping with CDCl<sub>3</sub>), 3.92 (s, 3H), 3.62 (m, 2H), 3.54 (m, 6H), 1.49 (s, 9H). <sup>13</sup>C NMR (500 MHz, CDCl<sub>3</sub>) δ 161.1, 159.7, 155.6, 154.6, 153.6, 152.5, 152.2, 145.5, 129.3, 126.7, 124.1, 119.8, 115.6, 113.1, 101.0, 80.4, 56.2, 44.8, 44.1, 28.4; ESI-HRMS, negative mode: *m/z* calcd mass for C<sub>24</sub>H<sub>25</sub>F<sub>3</sub>N<sub>6</sub>O<sub>6</sub>S [M - H]<sup>-</sup> = 581.1436, was found 581.143.

(*E*)-4-((4-(2-Cyano-3-oxo-3-((5-(trifluoromethyl)-1,3,4-thiadiazol-2-yl)amino)prop-1-en-1-yl)-2-methoxyphenoxy)carbonyl)piperazin-1-ium 2,2,2-trifluoroacetate, **13**. TFA (0.4 mL, 5.24 mmol) in DCM (0.4 mL) was added dropwise to a stirred solution of **12** (50 mg, 0.086 mmol) in dry DCM (0.8 mL) under argon, at 0 °C. The reaction mixture was then stirred at 0 °C for 1 h. The solvent was removed under reduced pressure, and the resulting TFA salt was washed with DCM and DCM–acetone (5:1) mixture. The obtained yellow white solid (50 mg, 98%) was used in subsequent reactions without any further purification. **13**: <sup>1</sup>H NMR (500 MHz, DMSO-*d*<sub>6</sub>) δ 9.01 (s, 2H), 8.53 (s, 1H), 7.80 (d, *J* = 1.6 Hz, 1H), 7.66 (dd, *J* = 8.4, 1.6 Hz, 1H), 7.39 (d, *J* = 8.3 Hz, 1H), 3.87 (s, 3H), 3.82 (m, 2H), 3.65 (m, 2H), 3.22 (s, 4H). <sup>13</sup>C NMR (126 MHz, DMSO-*d*<sub>6</sub>) δ 165.6, 164.4, 152.3, 152.3, 151.8, 149.8, 143.6, 130.6, 124.4, 124.2, 120.5, 116.5, 114.6, 106.8, 56.5, 42.9, 41.9, 41.2; ESI-MS, negative mode: *m/z* calcd mass for C<sub>19</sub>H<sub>17</sub>F<sub>3</sub>N<sub>6</sub>O<sub>4</sub>S [M - H]<sup>-</sup> = 481.0911, was found 481.0908.

bis(2,5-Dioxopyrrolidin-1-yl) glutarate, **15**. EDCi (290 mg, 1.51 mmol) was added to a solution of glutaric acid (100 mg, 0.757 mmol) and NHS (232 mg, 2.01 mmol) in 10 mL of dry DMF over 5 min. The reaction mixture was stirred overnight, and the solvent was removed under reduced pressure. The residue was taken up in EtOAc and transferred to a separatory funnel. The organic phase was washed (1N HCl, brine, sat. NaHCO<sub>3</sub>, brine) and dried with Na<sub>2</sub>SO<sub>4</sub>. The combined organic layers were concentrated under vacuum to yield a white solid, which was then resuspended in 2-propanol and stirred for 20 min. The resultant solid was filtered, washed with 2-propanol, and collected to yield the desired **15** (220 mg, 89%) without any further purification. **15**: <sup>1</sup>H NMR (500 MHz, CDCl<sub>3</sub>) δ 2.84 (m, 8H), 2.79 (m, 4H), 2.19 (m, 2H); <sup>13</sup>C NMR (500 MHz, CDCl<sub>3</sub>) δ 169.1, 167.8, 29.8, 25.7, 19.8.

(E)-4-(2-Cyano-3-oxo-3-((5-(trifluoromethyl)-1,3,4-thiadiazol-2-yl)amino)prop-1-en-1-yl)-2-methoxyphenyl 4-(5-((2,5-dioxopyrrolidin-1-yl)oxy)-5-oxopentanoyl)piperazine-1-carboxylate, **16**. Triethylamine (23 μg, 0.168 mmol) was added to a stirred solution of bis(2,5-dioxopyrrolidin-1-yl) glutarate (16.4 mg, 0.050 mmol) and **13** (25 mg, 0.042 mmol) in anhydrous DMF (0.7 mL) under argon. The reaction was then stirred at room temperature overnight. The solvent was removed under vacuum, and the residue was chromatographed on silica gel (eluent: DCM/acetone = 4/0.5 then DCM/MeOH = 5/0.1 to 5/4) to afford **16** (13 mg, 45%) as a white solid. **16**: <sup>1</sup>H NMR (500 MHz, DMSO-*d*<sub>6</sub>) δ 8.56 (s, 1H), 7.79 (d, *J* = 1.7 Hz, 1H), 7.66 (dd, *J* = 8.4, 1.7 Hz, 1H), 7.39 (d, *J* = 8.3 Hz, 1H), 3.86 (s, 3H), 3.66–3.41 (m, 10H), 2.82 (brs, 4H), 2.75 (t, *J* = 7.3 Hz, 2H), 1.88 (m, 2H); <sup>13</sup>C NMR (126 MHz, DMSO-*d*<sub>6</sub>) δ 170.7, 170.4, 169.3, 164.0, 153.1, 152.5, 151.9, 144.2, 130.2, 124.6, 124.4, 120.4, 116.2, 114.6, 109.9, 105.7, 56.4, 44.8, 44.2, 43.9, 41.1, 31.1, 30.1, 25.9, 20.5; ESI-MS, negative mode: *m/z* calcd mass for C<sub>28</sub>H<sub>26</sub>F<sub>3</sub>N<sub>7</sub>O<sub>9</sub>S [M – H]<sup>–</sup> = 692.15, was found 691.90.

Conjugate **geo41**. DIEA (1.4 μL, 7.75 μmol) was added to a stirred solution of **16** (2 mg, 2.9 μmol) and c(RGDyK) (1.2 mg, 1.94 μmol) in dry DMF (0.6 mL) under argon, and the mixture was stirred at room temperature for 2 days. The solvent was removed under reduced pressure, and the residue was purified with HPLC (gradient 90% H<sub>2</sub>O (0.1% FA)–10% ACN (0.1% FA)) to afford **geo41** as a white solid in 47% yield. **geo41**: <sup>1</sup>H NMR (500 MHz, DMSO-*d*<sub>6</sub>) δ 9.13 (s, 1H), 8.33 (d, *J* = 3.6 Hz, 1H), 8.28 (s, 1H), 8.14 (s, 1H), 8.12 (d, *J* = 8.8 Hz, 1H), 8.04 (d, *J* = 7.7 Hz, 1H), 7.82 (m, 2H), 7.78 (d, *J* = 1.7 Hz, 2H), 7.61 (dd, *J* = 8.4, 1.7 Hz, 2H), 7.26 (d, *J* = 8.3 Hz, 1H), 6.91 (d, *J* = 8.4 Hz, 2H), 6.60 (d, *J* = 8.4 Hz, 2H), 4.47 (s, 1H), 4.38 (q, *J* = 7.1 Hz, 1H), 4.23 (s, 1H), 4.05 (dd, *J* = 15.3, 8.1 Hz, 1H), 4.00 (s, 1H), 3.82 (s, 3H), 3.52 (m, 8H), 3.07 (m, 2H), 2.96 (m, 2H), 2.88 (s, 1H), 2.66–2.59 (m, 2H), 2.32 (t, *J* = 7.4 Hz, 2H), 2.17–2.03 (m, 2H), 1.78–1.61 (m, 2H), 1.59–1.00 (m, 12H); <sup>13</sup>C NMR (126 MHz, DMSO-*d*<sub>6</sub>) δ 172.2, 172.1, 171.8, 171.7, 171.1, 170.8, 170.6, 170.2, 168.9, 166.8, 163.4, 156.6, 155.7, 152.3, 151.3, 147.9, 146.5, 142.3, 131.2, 129.9, 127.6, 123.7, 122.8, 121.4, 118.0, 114.9, 114.0, 111.9, 55.9, 54.7, 54.3, 51.6, 48.8, 44.6, 44.4, 43.1, 40.7, 40.4, 38.8, 36.4, 34.7, 31.8, 31.1, 28.6, 28.1, 25.1, 22.9, 20.9; ESI-HRMS, negative mode: *m/z* calcd mass for C<sub>51</sub>H<sub>62</sub>F<sub>3</sub>N<sub>15</sub>O<sub>14</sub>S [M + H]<sup>–</sup> = 1196.4201, was found 1196.4171.

2-(2-(2-Hydroxyethoxy)ethoxy)ethyl methanesulfonate, **S4**. Methanesulfonyl chloride (400 mg, 3.50 mmol) was added dropwise to a stirred solution of triethylene glycol (500 mg, 3.33 mmol) and triethylamine (371 mg, 3.66 mmol) in dry

dichloromethane (6.25 mL) under argon at 0 °C. The reaction mixture was stirred at 0 °C for 1 h, and the reaction was quenched with water. Subsequently, the product was extracted with dichloromethane. The organic layers were dried over Na<sub>2</sub>SO<sub>4</sub>, filtered, and concentrated under reduced pressure. The crude residue was purified by column chromatography (eluent; EtOAc/MeOH = 100/2 to 100/10) to yield 173 mg of **S4** (23%) as a slightly yellow oil.<sup>22</sup> **S4**: <sup>1</sup>H NMR (500 MHz, CDCl<sub>3</sub>) δ 4.41–4.37 (m, 2H), 3.80–3.77 (m, 2H), 3.74 (s, 2H), 3.69 (d, *J* = 4.2 Hz, 4H), 3.64–3.59 (m, 2H), 3.08 (s, 3H), 2.17 (s, 1H).

2-(2-(2-Iodoethoxy)ethoxy)ethanol, **S5**. Sodium iodide (254 mg, 1.7 mmol) was added to a stirred solution of mesylated compound **S4** (173 mg, 0.76 mmol) in dry acetone (1.62 mL) under argon. The mixture was refluxed for 2 h in the dark. The solvent was removed under reduced pressure, and the crude residue was extracted with ethyl acetate (2 × 10 mL). The combined extracts were first washed with 10% Na<sub>2</sub>S<sub>2</sub>O<sub>3</sub>, then with brine, and dried over Na<sub>2</sub>SO<sub>4</sub>. The crude residue was purified by column chromatography over silica gel (eluent: CHCl<sub>3</sub>/MeOH = 100/1) to afford the desired iodide derivative **S5** (178 mg, 90%) as a colorless liquid.<sup>29</sup> **S5**: <sup>1</sup>H NMR (500 MHz, CDCl<sub>3</sub>) δ 3.79–3.75 (m, 2H), 3.74 (d, *J* = 5.6 Hz, 2H), 3.71–3.66 (m, 4H), 3.65–3.61 (m, 2H), 3.27 (t, *J* = 6.8 Hz, 2H), 2.17 (t, *J* = 6.2 Hz, 1H).

(E)-2-Cyano-3-(4-(2-(2-(2-hydroxyethoxy)ethoxy)ethoxy)-3-methoxyphenyl)-N-(5-(trifluoromethyl)-1,3,4-thiadiazol-2-yl)acrylamide, **18**. K<sub>2</sub>CO<sub>3</sub> (90 mg, 0.65 mmol) was added to a stirring solution of SRPIN803 (120 mg, 0.32 mmol) in dry DMF (3.6 mL), followed by 2-(2-(2-iodoethoxy)ethoxy)ethanol **S2** (169 mg, 0.65 mmol) at room temperature under argon atmosphere. The reaction mixture was refluxed overnight at 65 °C in the dark. After cooling to room temperature, the suspension was filtered and the filtrate was concentrated. The crude residue was purified by column chromatography (eluent: DCM/acetone = 4/0.5 to 4/2, then DCM/MeOH = 10/0.3 to 10/2) to give compound **18** as a yellow solid (130 mg, 80%). **geo33**: <sup>1</sup>H NMR (500 MHz, acetone-*d*<sub>6</sub>) δ 8.50 (s, 1H), 7.85 (d, *J* = 1.1 Hz, 1H), 7.67 (dd, *J* = 8.3, 1.2 Hz, 1H), 7.18 (d, *J* = 8.5 Hz, 1H), 4.32–4.28 (m, 2H), 3.93–3.88 (m, 5H), 3.73–3.70 (m, 2H), 3.67–3.63 (m, 4H), 3.55 (t, *J* = 5.0 Hz, 2H); <sup>13</sup>C NMR (126 MHz, acetone-*d*<sub>6</sub>) δ 163.2, 163.0, 153.5, 153.5, 151.1, 149.5, 127.4, 124.7, 120.3, 116.0, 112.8, 112.7, 101.2, 72.6, 70.5, 70.2, 69.1, 68.5, 61.0, 55.3; ESI-HRMS direct ionization, negative mode: *m/z* calcd mass for C<sub>20</sub>H<sub>21</sub>F<sub>3</sub>N<sub>4</sub>O<sub>6</sub>S [M – H]<sup>–</sup> = 501.1061, was found 501.1041.

(E)-2-(2-(2-(4-(2-Cyano-3-oxo-3-((5-(trifluoromethyl)-1,3,4-thiadiazol-2-yl)amino)prop-1-en-1-yl)-2-methoxyphenoxy)ethoxy)ethoxy)ethyl (4-nitrophenyl) carbonate, **19**. 4-Nitrophenyl chloroformate (6 mg, 0.03 mmol) was added to a stirred solution of **18** (10 mg, 0.02 mmol) in dry DMF (0.37 mL) and triethylamine (8 mg, 0.08 mmol), at 0 °C, under argon. After the addition of 4-nitrophenyl chloroformate, the solution turned orange and the mixture was left under stirring at room temperature for 3 h. Then, the solvent was removed under reduced pressure and the residue was chromatographed on silica gel (eluent: DCM/acetone = 4/2) to give **19** (10 mg, 75% yield) as a yellow solid. **19**: <sup>1</sup>H NMR (500 MHz, acetone-*d*<sub>6</sub>) δ 8.49 (s, 1H), 8.37–8.25 (m, 2H), 7.88 (d, *J* = 2.0 Hz, 1H), 7.70 (dd, *J* = 8.5, 2.0 Hz, 1H), 7.60–7.49 (m, 2H), 7.22 (d, *J* = 8.5 Hz, 1H), 4.46–4.37 (m, 2H), 4.35–4.29 (m, 2H), 3.93 (m, 2H), 3.91 (s, 3H), 3.84–3.77 (m, 2H), 3.74 (dd, *J* = 5.8, 3.0 Hz, 2H), 3.69 (dd, *J* = 5.9, 3.2 Hz, 2H); <sup>13</sup>C NMR (126

MHz, acetone- $d_6$ )  $\delta$  163.5, 163.5, 156.8, 154.9, 154.8, 153.4, 152.4, 150.7, 146.5, 128.5, 126.1, 125.6, 123.2, 120.2, 116.8, 113.8, 113.8, 101.5, 71.6, 71.3, 70.2, 69.6, 69.4, 69.3, 56.3; ESI-HRMS direct ionization, negative mode:  $m/z$  calcd mass for  $C_{27}H_{24}F_3N_5O_{10}S$   $[M - H]^- = 666.1123$ , was found 666.1110.

**Conjugate geo35.** DIEA (1.08 mg, 0.008 mmol) was added to a stirred solution of **19** (1.68 mg, 0.003 mmol) and c(RGDyK) (1.3 mg, 0.002 mmol) in dry DMF (0.52 mL) under argon, and the mixture was stirred at room temperature for 2 days. The solvent was removed under reduced pressure, and the residue was purified by reversed-phase HPLC to yield **19** as green-yellow solid (0.9 mg, 40%). The purity of the conjugate was confirmed by LC-MS and mass spectrometry (linear gradient from 90%  $H_2O$  to 10% acetonitrile, HCOOH 0.1%, over 30 min, flow rate: 0.4 mL/min, Rt = 19.3 min). **geo35:**  $^1H$  NMR (500 MHz, DMSO- $d_6$ )  $\delta$  9.14 (s, 1H), 8.34 (s, 1H), 8.23 (s, 1H), 8.17 (s, 1H), 8.13 (d,  $J = 8.7$  Hz, 1H), 8.06 (d,  $J = 7.2$  Hz, 1H), 7.85 (d,  $J = 7.3$  Hz, 1H), 7.79 (br, 1H), 7.76 (d,  $J = 2.0$  Hz, 1H), 7.64 (br, 1H), 7.60 (dd,  $J = 1.82, 8.61$  Hz, 1H), 7.19 (t,  $J = 5.6$  Hz, 1H), 7.14 (d,  $J = 8.6$  Hz, 2H), 6.92 (d,  $J = 8.5$  Hz, 2H), 6.62 (d,  $J = 8.5$  Hz, 2H), 4.51 (s, 1H), 4.39 (dd,  $J = 14.5, 7.4$  Hz, 1H), 4.31–4.13 (m, 3H), 4.11–3.93 (m, 4H), 3.83 (s, 3H), 3.81–3.75 (m, 2H), 3.68–3.50 (m, 5H), 3.28–3.20 (m, 2H), 3.09 (m, 2H), 2.91 (m, 4H), 2.64 (m, 1H), 2.47 (m, 2H), 1.77–1.64 (m, 2H), 1.54 (m, 2H), 1.48–1.18 (m, 6H), 1.09 (s, 2H);  $^{13}C$  NMR (126 MHz, DMSO- $d_6$ )  $\delta$  172.1, 171.9, 171.1, 170.8, 170.2, 169.0, 167.3, 156.6, 156.2, 155.7, 150.9, 148.7, 148.5, 146.3, 129.9, 127.5, 125.6, 124.8, 121.2, 118.6, 114.9, 112.8, 112.6, 108.9, 69.9, 69.7, 68.9, 68.8, 67.9, 63.1, 55.5, 54.7, 54.3, 51.6, 48.8, 43.2, 40.4, 36.5, 31.1, 28.9, 28.1, 25.0, 22.8 (2 carbons are missing due to overlapping); ESI-HRMS, negative mode:  $m/z$  calcd mass for  $C_{48}H_{60}N_{13}O_{15}S$   $[M + H]^- = 1146.3932$ , was found 1146.3906.

**Chemostability Assay.** The stability of the conjugates was examined by performing chemostability tests at two different pH values, 7.4 and 5.2. Stock solutions of the conjugates were prepared (0.32–0.47 mM) by dissolving 0.19–0.28 mg of each conjugate with 5  $\mu$ L of DMSO and 500  $\mu$ L of the relevant buffer solution (phosphate buffer pH 7.4 or acetate buffer pH 5.2). The solution was incubated at 37 °C. Aliquots were collected at 0, 1, 3, 5, 7, 24, and 48 h and analyzed by LC-MS. Results are presented as mean  $\pm$  SD for three independent experiments.

**Biostability Assay in Human Plasma.** c(RGDyK)-based conjugates (250  $\mu$ g dissolved in 5  $\mu$ L of DMSO) were added to 0.5 mL of human plasma. Solutions were maintained at 37 °C, and at predetermined time points (0.25 + 0, 1, 2, 3, 4, 5, 24, and 48 h), 50  $\mu$ L of aliquot was removed and quenched with 150  $\mu$ L of ice-cold acetonitrile (+0.1% formic acid) and centrifuged at 10 000 rpm for 10 min. Supernatant (50  $\mu$ L) was added to 50  $\mu$ L of ultrapure water (+0.1% formic acid) and analyzed by LC-MS. Results are presented as mean  $\pm$  SD for three independent experiments.

**Biostability Assay in Dulbecco's Modified Eagle's Medium.** c(RGDyK)-based conjugates (200  $\mu$ g dissolved in 5  $\mu$ L of DMSO) were added to 0.5 mL of DMEM (+ 10% fetal bovine serum). Solutions were maintained at 37 °C and at predetermined time points (0, 1, 2, 3, 4, 5, 24, 48, and 72 h), 50  $\mu$ L of aliquot was removed and quenched with 150  $\mu$ L of acetonitrile/ $H_2O$ :1:1 v/v solution (+0.1% formic acid) and analyzed by LC-MS. Results are presented as mean  $\pm$  SD for three independent experiments.

**Molecular Docking Studies.** SRPK1 complexed to SRPIN340 (PDB ID: 4WUA) and the crystal structure of

CK2 $\alpha$  (PDB ID: 6RB1) complexed to SRPIN803 were used as the protein models after removal of the ligand, water, and inhibitor molecules. During docking, nonpolar hydrogens were merged, and polar hydrogens and Gasteiger charges were added using AutoDock Tools 1.5.6. The ligands were drawn and energy-minimized in Chem3D 15.0. The computational docking analysis was performed using AutoDock Vina integrated in PyRx and BIOVIA Discovery Studio to visualize the results. Prior to docking experiments, the grid boxes were adjusted with volumetric spaces of 31x23x20 (Å) and 25x23x27 (Å) for SRPK1 and CK2 proteins, respectively, around the ATP binding sites of both kinases, and the "exhaustiveness" was set to 100. The docking poses with the lowest binding affinity were considered as the most favorable docking pose for presentation.

**In Vitro Kinase Assays.** Human SRPK1 and a fragment of the N-terminal domain of turkey Lamin B Receptor (LBR) comprising amino acids 62–92 (LBRNt(62–92)) were subcloned into pGEX-2T and expressed in bacteria as GST fusion proteins as previously described.<sup>23</sup> Kinase assays were performed in a reaction mixture containing 0.5  $\mu$ g of GST-SRPK1, 1.5  $\mu$ g of GST-LBRNt(62–92) as a substrate, 25  $\mu$ M ATP, 1  $\mu$ Ci of [ $\gamma$ - $^{32}P$ ]ATP, 12 mM Hepes pH 7.5, 10 mM  $MgCl_2$ , and the appropriate amount of the inhibitor in a final volume of 25  $\mu$ L. Reactions were carried out for 30 min at 30 °C. The final concentration of dimethyl sulfoxide (DMSO) was adjusted to 4% irrespectively of the inhibitor concentration.

Human recombinant casein kinase 2 (CK2) was purchased from New England Biolabs. The CK2 kinase assay was performed in a reaction mixture containing 100 units of CK2, 1.5  $\mu$ g of dephosphorylated casein (Sigma), 25  $\mu$ M ATP, 1  $\mu$ Ci of [ $\gamma$ - $^{32}P$ ]ATP, 50 mM Tris-HCl pH 7.5, 10 mM  $MgCl_2$ , and the appropriate amount of the inhibitor in a final volume of 25  $\mu$ L. Reactions were carried out for 30 min at 30 °C. The final concentration of dimethyl sulfoxide (DMSO) was adjusted to 4% irrespectively of the inhibitor concentration. Phosphoproteins were detected by autoradiography using Super RX (Fuji medical X-ray film), and incorporation of radioactivity was measured by excising the radioactive bands from the SDS-PAGE gel and scintillation counting.

**MTT Assays.** The cells were plated in a 96-well plate at a density of  $1 \times 10^4$  cells/mL and maintained for 72 h at 37 °C in a 5%  $CO_2$  incubator and cultured as monolayers. After 24 h, the cells were treated with 0.1–100  $\mu$ mol/L of the tested compounds for 48 h. Following 48 h of drug exposure, cell viability was determined by the MTT metabolic assay as described previously.<sup>30</sup> (4,5-Imethylthiazol-2-yl)-2,5-diphenyl-tetrazolium bromide (MTT, Sigma, MO) was dissolved in PBS in a concentration of 5 mg/mL and added to the cultured cells. After 3 h of incubation at 37 °C, formazan crystals were solubilized by DMSO (100  $\mu$ L). The absorbance of the converted dye was measured at a wavelength of 540 nm on an ELISA reader (VersaMax, CA). The percentage growth inhibition was calculated according to National Cancer Institute recommendations as:  $[(Tt72x) - (Ct24)/(Ct72) - (Ct24)] \times 100$  for concentrations for which  $Tt72x > Ct24$  and  $[(Tt72x) - (Ct24)/Ct24] \times 100$  for concentrations for which  $Tt72x < Ct24$ .  $GI_{50}$  was calculated from  $[(Tt72x) - (Ct24)/(Ct72) - (Ct24)] \times 100 = 50$ , total growth inhibition (TGI) from  $[(Tt72x) - (Ct24)/(Ct72) - (Ct24)] \times 100 = 0$ , and 50% growth inhibition ( $IC_{50}$ ) from  $[(Tt72x) - (Ct24)/Ct24] \times 100 = 50$ . All of the experiments were carried out in triplicate.

**Zebrafish Screening Assays.** Maintenance and breeding of the *Tg(kdrl:gfp)* zebrafish transgenic line was carried out in

accordance with the European Directive 2010/63 for the protection of animals used for scientific purposes and the Recommended Guidelines for Zebrafish Husbandry Conditions.<sup>31</sup> Only embryos up to 72 h post fertilization were used in these experiments. For the compound treatment assay: Zebrafish embryos were raised in E3 medium up to 24hpf; they were then dechlorinated and transferred to a 12-well plate (10 embryos/well). Candidate compounds were initially dissolved in DMSO and added at E3 medium (containing phenylthiourea, PTU) at a 100  $\mu$ M final concentration. Treated and DMSO control embryos were kept at 28 °C and imaged at 72hpf. For the microinjections: zebrafish *Tg(kdrl:gfp)* embryos were injected at one-cell stage with 4.6 nL of 10  $\mu$ M of each compound/embryo and were kept in E3 medium at 28 °C up to 72hpf.

**Zebrafish Imaging Analysis.** Embryos were anesthetized with 0.4% tricaine methanesulfonate (MS222), and images were acquired by Leica DMIRE2 with a mounted Hamamatsu ORCA-Flash4.0LT digital camera. For quantification of the antiangiogenic effect of compounds, the total length of 10 intersegmental vessels (ISVs) per embryo flanking the yolk extension was measured using the open-source software ImageJ 1.52p (<http://imagej.nih.gov/ij>). A total of 30 embryos from independent experiments were measured. Statistically significant differences in total length were determined by a two-tailed Student's *t*-test, using GraphPad Prism 5.0, considering  $p^{***} < 0.001$ .

## ■ ASSOCIATED CONTENT

### SI Supporting Information

The Supporting Information is available free of charge at <https://pubs.acs.org/doi/10.1021/acsomega.1c04576>.

Detailed spectra for experimental characterization, LC-MS analysis, and docking studies (PDF)

## ■ AUTHOR INFORMATION

### Corresponding Author

Vasiliki Sarli – Department of Chemistry, Aristotle University of Thessaloniki, 54124 Thessaloniki, Greece; [orcid.org/0000-0002-6128-8277](https://orcid.org/0000-0002-6128-8277); Email: [sarli@chem.auth.gr](mailto:sarli@chem.auth.gr)

### Authors

George Leonidis – Department of Chemistry, Aristotle University of Thessaloniki, 54124 Thessaloniki, Greece  
Panagiotis Dalezis – Laboratory of Pharmacology, Medical School National and Kapodistrian University of Athens, Athens 11527, Greece  
Dimitrios Trafalis – Laboratory of Pharmacology, Medical School National and Kapodistrian University of Athens, Athens 11527, Greece  
Dimitris Beis – Zebrafish Disease Model Lab, Biomedical Research Foundation Academy of Athens, Athens 115 27, Greece; [orcid.org/0000-0003-2579-7848](https://orcid.org/0000-0003-2579-7848)  
Panagiota Giardoglou – Zebrafish Disease Model Lab, Biomedical Research Foundation Academy of Athens, Athens 115 27, Greece  
Anastasia Koukiali – Department of Chemistry, Aristotle University of Thessaloniki, 54124 Thessaloniki, Greece  
Ioanna Sigala – Department of Chemistry, Aristotle University of Thessaloniki, 54124 Thessaloniki, Greece  
Eleni Nikolakaki – Department of Chemistry, Aristotle University of Thessaloniki, 54124 Thessaloniki, Greece

Complete contact information is available at:

<https://pubs.acs.org/10.1021/acsomega.1c04576>

## Author Contributions

Program oversight and funding acquisition were performed under direction of V.S. Program conceptualization was done by Drs V.S. and E.N. Chemical synthesis was directed by V.S., with synthesis performed by G.L. Stability studies were performed by G.L. Computational modeling was directed by V.S., with modeling performed by G.L. Inhibition of kinase activity was directed by E.N., with assays performed by I.S. and A.K. Cytotoxicity study was directed by D.T. and E.N., performed by P.D., I.S., and A.K. Zebrafish angiogenesis was directed by D.B. and performed by P.G. Manuscript preparation and review were conducted by V.S. Correspondence with respect to chemical synthesis should be directed to V.S. Correspondence with respect to modeling should be directed to V.S. Correspondence with respect to pharmacological evaluations should be directed to E.N., D.B., and D.T.

## Notes

The authors declare no competing financial interest.

## ■ ACKNOWLEDGMENTS

This study was supported by the Hellenic Foundation for Research and Innovation (H.F.R.I.) under the 'First Call for H.F.R.I. Research Projects to support Faculty members and Researchers and the procurement of high-cost research equipment grant' (Project Number:12), Title: Synthesis and biological evaluation of RGD-conjugated SRPK1 kinase inhibitors for integrin-targeted cancer therapy.

## ■ REFERENCES

- (1) Risau, W. Mechanisms of angiogenesis. *Nature* **1997**, *386*, 671–674.
- (2) Yoo, S. Y.; Kwon, S. M. Angiogenesis and its therapeutic opportunities. *Mediators Inflamm.* **2013**, *2013*, 1–11.
- (3) Fidler, I. J. Angiogenesis and cancer metastasis. *Cancer J.* **2000**, *6*, 134–141.
- (4) Maruotti, N.; Cantatore, F.; Crivellato, E.; Vacca, A.; Ribatti, D. Angiogenesis in rheumatoid arthritis. *Histol. Histopathol.* **2006**, *21*, 557–566.
- (5) Martin, A.; Komada, M. R.; Sane, D. C. Abnormal angiogenesis in diabetes mellitus. *Med. Res. Rev.* **2003**, *23*, 117–145.
- (6) Jayson, G. C.; Kerbel, R.; Ellis, L. M.; Harris, A. L. Antiangiogenic therapy in oncology: current status and future directions. *Lancet* **2016**, *388*, 518–529.
- (7) Nieberler, M.; Reuning, U.; Reichart, F.; Notni, J.; Wester, H. J.; Schwaiger, M.; Weinmüller, M.; Räder, A.; Steiger, K.; Kessler, H. Exploring the Role of RGD-Recognizing Integrins in Cancer. *Cancers* **2017**, *9*, No. 116.
- (8) Soldi, R.; Mitola, S.; Strasly, M.; Defilippi, P.; Tarone, G.; Bussolino, F. Role of  $\alpha$ v $\beta$ 3 integrin in the activation of vascular endothelial growth factor receptor-2. *EMBO J.* **1999**, *18*, 882–892.
- (9) Cornel, S.; Adriana, I. D.; Mihaela, T. C.; Speranta, S.; Algerino, DeS.; Mehdi, B.; Jalaladi, H.-R. Anti-vascular endothelial growth factor indications in ocular disease. *Rom. J. Ophthalmol.* **2015**, *59*, 235–242.
- (10) Amin, E. M.; Oltean, S.; Hua, J.; Gammons, M. V.; Hamdollah-Zadeh, M.; Welsh, G. I.; Cheung, M. K.; Ni, L.; Kase, S.; Rennel, E. S.; Symonds, K. E.; Nowak, D. G.; Royer-Pokora, B.; Saleem, M. A.; Hagiwara, M.; Schumacher, V. A.; Harper, S. J.; Hinton, D. R.; Bates, D. O.; Ladomery, M. R. WT1 mutants reveal SRPK1 to be a downstream angiogenesis target by altering VEGF splicing. *Cancer Cell* **2011**, *20*, 768–780.
- (11) Fukuhara, T.; Hosoya, T.; Shimizu, S.; Sumi, K.; Oshiro, T.; Yoshinaka, Y.; Suzuki, M.; Yamamoto, N.; Herzenberg, L. A.; Herzenberg, L. A.; Hagiwara, M. Utilization of host SR protein kinases

- and RNA-splicing machinery during viral replication. *Proc. Natl. Acad. Sci. U.S.A.* **2006**, *103*, 11329–11333.
- (12) Gammons, M. V.; Dick, A. D.; Harper, S. J.; Bates, D. O. SRPK1 inhibition modulates VEGF splicing to reduce pathological neovascularization in a rat model of retinopathy of prematurity. *Invest. Ophthalmol. Vis. Sci.* **2013**, *54*, 5797–5806.
- (13) Morooka, S.; Hoshina, M.; Kii, I.; Okabe, T.; Kojima, H.; Inoue, N.; Okuno, Y.; Denawa, M.; Yoshida, S.; Fukuhara, J.; Ninomiya, K.; Ikura, T.; Furuya, T.; Nagano, T.; Noda, K.; Ishida, S.; Hosoya, T.; Ito, N.; Yoshimura, N.; Hagiwara, M. Identification of a Dual Inhibitor of SRPK1 and CK2 That Attenuates Pathological Angiogenesis of Macular Degeneration in Mice. *Mol. Pharmacol.* **2015**, *88*, 316–325.
- (14) Kramerov, A. A.; Saghizadeh, M.; Caballero, S.; Shaw, L. C.; Li Calzi, S.; Bretner, M.; Montenarh, M.; Pinna, L. A.; Grant, M. B.; Ljubimov, A. V. Inhibition of protein kinase CK2 suppresses angiogenesis and hematopoietic stem cell recruitment to retinal neovascularization sites. *Mol. Cell. Biochem.* **2008**, *316*, 177–186.
- (15) Qiao, Y.; Chen, T.; Yang, H.; Chen, Y.; Lin, H.; Qu, W.; Feng, F.; Liu, W.; Guo, Q.; Liu, Z. H.; et al. Sun Small molecule modulators targeting protein kinase CK1 and CK2. *Eur. J. Med. Chem.* **2019**, *181*, No. 111581.
- (16) Chatzisdieri, T.; Dalezis, P.; Leonidis, G.; Bousis, S.; Trafalis, D.; Bianchini, F.; Sarli, V. Synthesis and biological studies of c(RGDyK) conjugates of cucurbitacins. *Future Med. Chem.* **2021**, *13*, 877–895.
- (17) Chatzisdieri, T.; Thysiadis, S.; Katsamakas, S.; Dalezis, P.; Sigala, I.; Lazarides, T.; Nikolakaki, E.; Trafalis, D.; Gederaas, O. A.; Lindgren, M.; Sarli, V. Synthesis and biological evaluation of a Platinum(II)-c(RGDyK) conjugate for integrin-targeted photodynamic therapy. *Eur. J. Med. Chem.* **2017**, *141*, 221–231.
- (18) Giardoglou, P.; Beis, D. On Zebrafish Disease Models and Matters of the Heart. *Biomedicines* **2019**, *7*, No. 15.
- (19) Jin, S. W.; Beis, D.; Mitchell, T.; Chen, J. N.; Stainier, D. Y. R. Cellular and Molecular Analysis of Vascular Tube and Lumen Formation in Zebrafish. *Development* **2005**, *132*, 5199–5209.
- (20) Papakyriakou, A.; Kefalos, P.; Sarantis, P.; Tsiamantas, C.; Xanthopoulos, K. P.; Vourloumis, D.; Beis, D. A zebrafish in vivo phenotypic assay to identify 3-aminothiophene-2-carboxylic acid-based angiogenesis inhibitors. *Assay Drug Dev. Technol.* **2014**, *12*, 527–535.
- (21) Dalle Vedove, A.; Zonta, F.; Zanforlin, E.; Demitri, N.; Ribado, G.; Cazzanelli, G.; Ongaro, A.; Sarno, S.; Zagotto, G.; Battistutta, R.; Ruzzene, M.; Lolli, G. A novel class of selective CK2 inhibitors targeting its open hinge conformation. *Eur. J. Med. Chem.* **2020**, *195*, No. 112267.
- (22) Kumar, V.; Naika, V. G.; Dasb, A.; Bal, S. B.; Biswas, M.; Kumar, N.; Ganguly, A.; Chatterjee, A.; Banerjee, M. Synthesis of a series of ethylene glycol modified water-soluble tetrameric TPE-amphiphiles with pyridinium polar heads: Towards applications as light-up bioprobes in protein and DNA assay, and wash-free imaging of bacteria. *Tetrahedron* **2019**, *75*, 3722–3732.
- (23) Voukkalis, N.; Koutroumani, M.; Zarkadas, C.; Nikolakaki, E.; Vlassi, M.; Giannakouros, T. SRPK1 and Akt Protein Kinases Phosphorylate the RS Domain of Lamin B Receptor with Distinct Specificity: A Combined Biochemical and In Silico Approach. *PLoS One* **2016**, *11*, No. e0154198.
- (24) Trott, O.; Olson, A. J. AutoDock Vina: Improving the speed and accuracy of docking with a new scoring function, efficient optimization, and multithreading. *J. Comput. Chem.* **2010**, *31*, 455–461.
- (25) Park, K.-Y.; Kim, J. Cyclic pentapeptide cRGDFK enhances the inhibitory effect of sunitinib on TGF- $\beta$ 1-induced epithelial-to-mesenchymal transition in human non-small cell lung cancer cells. *PLOS ONE* **2020**, *15*, No. e0232917.
- (26) Hong, K.-H.; Kim, D. I.; Kwon, H.; Kim, H. J. A fluoresceinylcarbonate-based fluorescent probe for the sensitive detection of biothiols in a HEPES buffer and its cellular expression. *RSC Adv.* **2014**, *4*, 978–982.
- (27) Favre, A.; Grugier, J.; Brans, A.; Joris, B.; Marchand-Brynaert, J. Aminopenicillanic acid (6-APA) derivatives equipped with anchoring arms. *Tetrahedron* **2012**, *68*, 10818–10826.
- (28) Cheng, C.; Sun, J.; Xing, L.; Xu, J.; Wang, X.; Hu, Y. Highly chemoselective Pd-C catalytic hydrodechlorination leading to the highly efficient N-debenzylation of benzylamines. *J. Org. Chem.* **2009**, *74*, 5671–5674.
- (29) Tian, T.; Qian, T.; Jiang, T.; Deng, Y.; Li, X.; Yuan, W.; Chen, Y.; Hu, W.; Wang, Y. X. A donor–acceptor type macrocycle: toward photolyzable self-assembly. *Chem. Commun.* **2020**, *56*, 3939–3942.
- (30) Sigala, I.; Tsamis, K. I.; Gousia, A.; Alexiou, G.; Voulgaris, S.; Giannakouros, T.; Kyritsis, A. P.; Nikolakaki, E. Expression of SRPK1 in gliomas and its role in glioma cell lines viability. *Tumour Biol.* **2016**, *37*, 8699–8707.
- (31) Aleström, P.; D’Angelo, L.; Midtlyng, P. J.; Schorderet, D. F.; Schulte-Merker, S.; Sohm, F.; Warner, S. Zebrafish: Housing and husbandry recommendations. *Lab Anim.* **2020**, *54*, 213–224.